Analysis of nonlinear responses of asphalt pavements under overloading and tropical climate temperature conditions

Kumar, Abhinav; Gupta, Ankit; Anupam, Kumar; Premarathna, W. A.A.S.

DOI
10.1016/j.cscm.2025.e04760

Publication date
2025

Document Version
Final published version

Published in
Case Studies in Construction Materials

Citation (APA)
Kumar, A., Gupta, A., Anupam, K., & Premarathna, W. A. A. S. (2025). Analysis of nonlinear responses of asphalt pavements under overloading and tropical climate temperature conditions. *Case Studies in Construction Materials*, *22*, Article e04760. https://doi.org/10.1016/j.cscm.2025.e04760

Case Studies in Construction Materials 22 (2025) e04760

Contents lists available at ScienceDirect

Case Studies in Construction Materials

journal homepage: www.elsevier.com/locate/cscm

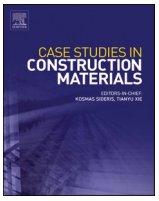

Analysis of nonlinear responses of asphalt pavements under overloading and tropical climate temperature conditions

Abhinav Kumar [a], Ankit Gupta [a], Kumar Anupam [b,*], W.A.A.S. Premarathna [b]

[a] Department of Civil Engineering, IIT BHU, Varanasi, India
[b] Department of Civil Engineering & Geoscience, Delft University of Technology, Delft, the Netherlands

ARTICLE INFO

Keywords:
Creep compliance
Resilient modulus
Stress dependent behaviour
FE modelling
Overloading

ABSTRACT

The design of asphalt pavement in many developing nations still relies on an empirical approach, often leading to either premature failure of the pavement or overdesign. The transition from an empirical approach to semi-mechanistic or mechanistic was felt by past researchers, and many advanced tools based on these approaches have been developed. Computational tools, like finite element (FE) analysis, are capable of handling complex material properties of pavement materials under nonuniform loading conditions. Asphalt mixes are widely known to exhibit viscoelastic behaviour based on temperature and loading conditions, while the response of unbound materials under cyclic loading is stress dependent. Due to the complexity of the entire process, numerous pavement design tools treat them as purely elastic materials. This study aims to develop a finite element based, simple, and practical framework to assess the structural response of asphalt pavement under overloading and varying temperature conditions in a tropical climate. The framework offers a straightforward method for the determination of time dependent viscoelastic parameters of the asphalt mixture using creep compliance test. The nonlinear stress-dependent behaviour of unbound granular materials (UGMs) in different layers has also been presented based on repeated load triaxial compression testing. It was concluded that overloading and increasing mix temperature severely affect pavement performance. A 25 % overloading resulted in a reduction of subgrade rutting life by 62.33 %, whereas an increase in mix temperature by 10° C at intermediate temperature reduced asphalt fatigue life by 29.34 % and subgrade rutting life by 42.03 %.

1. Introduction

Asphalt concrete (AC) pavements are considered mechanistically complex systems due to their composition of different materials and regular interaction with surrounding conditions [1]. Hence, their performance is influenced by parameters such as material properties, loading conditions, and environmental factors. In emerging economies like India, bituminous concrete (BC) is widely used as a surface layer in asphalt pavement. The Ministry of Road Transport & Highways (MoRTH) specifications [2] categorize BC based on their aggregate sizes. The first category, BC-1, is classified with a nominal aggregate size of 19 mm, whereas the second category, BC-2, is classified with a nominal aggregate size of 13.2 mm. Asphalt mixture in the asphalt concrete (AC) layer consists of aggregates, fillers, fibers, modifiers, air voids, and binders extracted as residuals in refineries [3]. Though different constituents present in the asphalt

* Corresponding author.
E-mail address: k.anupam@tudelft.nl (K. Anupam).

https://doi.org/10.1016/j.cscm.2025.e04760
Received 26 January 2025; Received in revised form 21 April 2025; Accepted 8 May 2025
Available online 9 May 2025

mixture exhibit substantially different properties, collectively, it can be categorized as a viscoelastic material [4–6]. The behaviour of these mixes can be considered as linear viscoelastic (LVE) subjected to small strain (less than 100 μm/m) amplitudes [7,8]. The strain amplitude is defined as half the difference between the maximum and minimum strain in a cyclic loading.

The viscoelastic properties of materials are typically characterized by measuring creep behaviour through a creep compliance test [9]. The elastic and viscoelastic strain response of the asphalt mix can be determined separately using these tests [10]. Creep compliance is defined as time dependent strain per unit applied stress, and it is a measurement of material deformation with time at different temperatures [26]. Besides temperature, creep compliance is also influenced by the properties of the constituents and their proportions in the asphalt mix. The effect of some of these aspects on the pavement response has been presented in this article.

Understanding the behaviour of asphalt mixes is crucial for performance-based design and is key to achieving the expected lifespan. Uncertainties (like material response to traffic loading subjected to different environmental conditions) during the mix design phase can lead to significant errors in lifespan estimation. Although the asphalt layer has a significant effect on the structural performance of the pavement as a major portion of the axle loading is absorbed in this layer itself; however, understanding material response to cyclic loading in lower layers is equally important for accurate estimation of the pavement response.

Typically, aggregates in the base and subbase layers and soil in the subgrade layer in untreated form are considered as UGMs. The response of these layers is often modelled as linear elastic [11], nonlinear elastic [12], or linear elastoplastic [13]. Unfortunately, the most commonly used layered elastic programs still consider the behaviour of these materials as linear elastic [14]. In reality, unbound materials are not truly elastic but experience some nonrecoverable deformation after each load repetition [15]. The increment in nonrecoverable deformation reduces after the first few cycles of loading as compared to increment in recoverable/resilient deformation [16]. Previous studies [17–21] have shown that the resilient behaviour of fine-grained subgrade soil and coarse-grained aggregate materials in base and subbase layers follows a nonlinear, stress-dependent response under repeated axle loading.

Various nonlinear constitutive models have been proposed by past researchers to explain the stress-dependent behaviour of unbound materials. Among nonlinear elastic models, a renowned stress-dependent model is the universal octahedral shear stress model [22], which accounts for the nonlinearity of these materials in a three-dimensional space. The plasticity of unbound materials has been modelled considering the classical plasticity criteria such as Drucker-Prager, Mohr-Coulomb, or Cam-Clay [23]. The American Association of State Highways and Transportation Officials (AASHTO) provides specifications for using stress-dependent nonlinear elastic properties of unbound materials. However, in India, pavement analysis and design as per IRC: 37 guidelines [24] are based on linear elastic properties of UGMs, which are derived empirically from soil CBR values. The current design procedure needs to incorporate nonlinear stress-dependent responses of UGMs to simulate material behaviour in the field. The layered elastic program, like IITPAVE for pavement design in India, is not built to consider the complex material properties of asphalt mixes and unbound materials. With advancements in computational facilities, such complicated problems can be adequately handled using finite element (FE) methods [25].

Other than material properties, loading and environmental conditions are considered as one of the crucial parameters affecting pavement performance and its life severely. Pavements are generally designed for a standard axle load. The cases of frequent overloading beyond the permissible limit pose serious concerns for pavement engineers in developing countries like India. Additionally, temperature is another important parameter that affects asphalt mix stiffness and its performance considerably, especially in tropical climate conditions. To the best of the authors' knowledge, limited studies are available that provide a framework to study the structural response of asphalt pavement under these conditions (overloading and tropical climate), considering complex material behaviour of asphalt mixes and UGMs and actual loading conditions.

In this study, a three-dimensional FE model of tire-pavement system using solid tire and deformable AC pavement was developed. The tire was modelled to consider nonuniform contact stress distribution at the tire-pavement interface. It is capable of assessing the structural behaviour of different pavement systems, considering time-dependent viscoelastic response of asphalt mixes and nonlinear stress-dependent behaviour of UGMs. It is noted that the proposed model is versatile, which can be recalibrated to the requirements of different road research agencies of the world. The Prony series parameters have been evaluated using nonlinear constrained optimization of creep compliance data predicted from GKM. These parameters have been further used as input parameters to represent the viscoelastic material properties of mixes in the FE model. The characterization of unbound granular layers is done by nonlinear resilient response based on triaxial compression testing. Hypoelastic modelling has been done to evaluate strain invariant parameters to be used as input parameters in the FE model. Since the commonly adopted circular contact area of uniform pressure distribution may not accurately reflect real field conditions, an actual solid tire was modelled at the tire-pavement interface. This study aims to understand the impact of overloading and tropical climate conditions on the structural response and pavement life.

1.1. Objective and scope of the study

This study aims to evaluate asphalt pavement response and its life in case of overloading and variable temperature conditions in tropical climates under nonuniform loading. A simplified framework for determining Prony series constants of the dense graded asphalt mixes has been discussed for the viscoelastic material characterization under Indian conditions. A creep compliance test was conducted to study viscoelastic response of asphalt mixes. The stress-dependent behaviour of unbound granular materials was presented using nonlinear constitutive models. These models are based on the resilient modulus data obtained from repeated load triaxial compression tests conducted on UGMs. A 3-dimensional FE model of tire-pavement system was developed in ABAQUS (FE software) that can capture the complex material behaviour in various layers under nonuniform loading conditions.

1.2. The novelty of the research

The novelty of the presented paper can be explained by the following key points:

1. The scope of the study: As discussed in the previous subsections, none of the existing studies provide a finite element-based framework that considers the complex material properties (viscoelastic response of asphalt mixes and nonlinear stress-dependent behaviour of UGMs) of pavement layers under nonuniform loading conditions for evaluating the structural response of the pavement subjected to overloading and temperature variations in the tropical climate.
2. Frictional properties at pavement layer interfaces: The novelty of this research lies in its comprehensive approach to simulating complex interactions at pavement layer interfaces. It enhances realism by incorporating tangential contact properties and friction coefficients derived from empirical testing, specifically through Newton's inclined plane test. This method allows for a more accurate reflection of actual field conditions.
3. Integration of complex material behaviour, interface mechanics, and loading conditions: The use of the Yeoh hyper-elastic material model for tire rubber adds depth to the analysis by providing a robust framework for understanding the mechanical behaviour of materials under stress. Overall, this research significantly advances the field of pavement engineering by integrating complex material behaviour, interface mechanics, and realistic simulation of loading conditions.
4. Structural response under overloading and variable temperature conditions: The mechanistic response of the asphalt pavement has been evaluated under overloading (25–100 %) and variable temperature in tropical climatic conditions like India, which has not been explored previously to the best of the authors' knowledge.

2. Methodology

This section summarizes the study's research methodology and a brief layout of the experimental plan to achieve the set objectives. The whole study is divided into four different steps. The first step deals with viscoelastic material characterization of asphalt mixes, in which time and temperature dependency of the material is evaluated using a creep compliance test. These creep compliance data were further converted to stress relaxation modulus. The Generalized Kelvin model was used to evaluate Prony series coefficients to be used as an input parameter in the FE model of asphalt pavement. The second step characterizes unbound granular materials (UGMs) based on resilient modulus test. The resilient modulus of UGMs was determined using repeated load triaxial compression testing, and various models were used to explain the stress dependency of these materials.

The third step involves finite element (FE) modelling of tire-pavement system. A finite element model of asphalt pavement and tire has been presented. A four-layer asphalt pavement system has been considered in the geometric design process. These layers include asphalt, base, subbase, and subgrade layer. The solid tire has been modelled to consider realistic nonuniform contact stress distribution at the tire-pavement interface. It is easy to evaluate the material properties of solid tire as it consists of a single rubber material. For modelling tire rubber, a suitable hyper-elastic material model was obtained using relevant tensile test data and a curve fitting approach [26]. Hyper-elastic models are generally used to calculate elastomer's properties that respond elastically when subjected to large

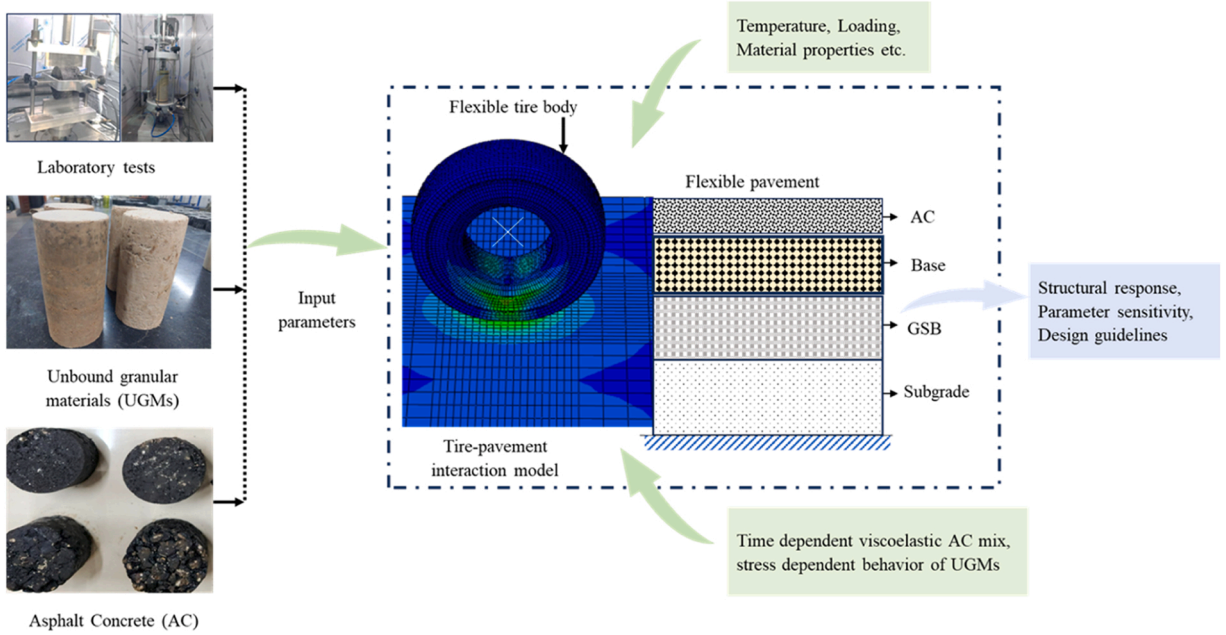

Fig. 1. Schematic of research methodology.

deformations [27].

The final step involves the evaluation of the structural response of the asphalt pavement under different conditions. The idea of study is to analyze the usefulness of the FE model of the tire-pavement system to (a) incorporate complex material properties of pavement layers, (b) consider nonuniform stress distribution in the loading area, and (c) explore the structural response of the pavement under different conditions. The developed FE model, after validation, is used to calculate horizontal tensile strain at the bottom of the asphalt layer and vertical compressive strain at the top of the subgrade layer. These strains are further used to compute pavement life in rutting and fatigue. These steps of research methodology are shown in Fig. 1.

3. Materials

Locally available soil and aggregate materials were used in this study. The silty soil of non-expensive nature was used as subgrade material. The maximum specified limit of free swelling index as per the standards [30] is 50 %. The maximum dry unit weight of the soil was found to be 18.75 kN/m^3, which is higher than the minimum specified value of 17.5 kN/m^3. The physical properties of binder to be used in the surface layer and aggregates for the granular subbase and base layer have been discussed in the following subsections.

3.1. Physical properties of binder

In the present study, VG-40 binder was used with an absolute viscosity of 4480 Poise at 60° C which falls within the specified limit of 3200–4800 Poise [28]. It is relatively a stiff binder generally used in roads designed to service higher axle loads. It is a common choice for the construction of major roadways such as national highways and expressways in India, expecting a load repetition of more than 30 million standard axles [29]. The use of VG-40 binder can be further extended, subjected to a maximum of 50 msa traffic load with a revised maximum pavement temperature of 64° C [2].

The binder properties were assessed before using them in the sample preparation and are shown in Table 1. As per Indian specifications [30], binders are classified based on viscosity, and there are no specific test protocols or specifications for performance grading and continuous grade at higher temperatures [31]. Therefore, ASTM guidelines [32] were followed to evaluate the rheological characteristics using a dynamic shear rheometer.

3.2. Physical properties of aggregates

In this study, Granite (a siliceous aggregate) was used for the preparation of bituminous mix samples. Granite is frequently used in the construction of flexible pavements in India. It produces a rough and angular texture, which improves interlocking between aggregate particles. Also, granite has high density and hardness, which adds structural integrity to the asphalt pavement. These strengths of granite aggregates make it a suitable choice for the construction of the base and asphalt layer. However, it shows poor adhesion to asphalt, which makes asphalt mixes susceptible to rainwater erosion. The adhesion between granite aggregates and asphalt can be improved with the use of additives and surface treatments to make it further suitable for the preparation of asphalt mixes. Prior to the preparation of the mix, the physical properties of the aggregates were examined, as shown in Table 2. As per the MoRTH [2] guidelines, combined flakiness and elongation index, abrasion value, and impact value tests of aggregates have been conducted to check the suitability of its usage in various layers of the AC pavement. Relevant IS codes, as mentioned in Table 2, have been used to conduct these physical tests on aggregate materials.

As granite aggregates are considered a very tough material in the construction of asphalt pavement, results of abrasion value and impact value tests confirm the same. These materials were found to be less susceptible to indentation and crushing, subjected to wearing action and impact loading. Test results shown in Table 2 mainly show the hardness, toughness, and shape properties of aggregates.

3.3. Physical properties of asphalt concrete mix

The dense graded bituminous mix (BC-2) was considered in this study, as it is widely used for the construction of flexible pavement in India. The aggregate gradation used in the preparation of BC-2 mixes is in accordance with MoRTH guidelines. The selected gradation and specification limits are shown in Fig. 2.

For preparing asphalt mixes, mid-point gradation has been selected in this study. Asphalt mixes were compacted at the design

Table 1
Specification limit and physical properties of binder.

Properties	Values obtained	Test method	Specification limit
Penetration at 25° C, 0.1 mm	41	IS 1203 [33]	35 (min)
Absolute viscosity at 60° C (Poises)	4480	IS 1206-Part 2 [28]	3200–4800
Softening point (°C)	54	IS 1205 [34]	50 (min)
High-temperature continuous grade (°C)	77.2	ASTM D6373 [32]	NA
High-temperature performance grade (°C)	76	ASTM D6373 [32]	NA

NA – Not applicable

Table 2
Specification limits and physical properties of aggregates.

Properties	Combined flakiness and elongation index	Abrasion value	Impact value
Specification limit	Max 35 %	Max 40 %	Max 30 %
Test protocol	IS:2386-Part I [35]	IS:2386-Part IV [36]	IS:2386-Part IV [36]
Test results	19 %	16.8 %	14.6 %

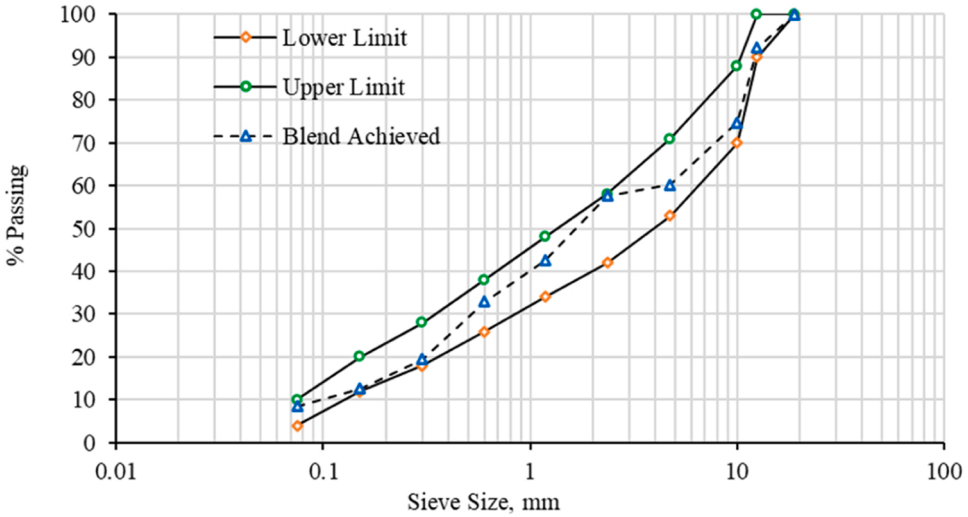

Fig. 2. Aggregate gradation adopted for BC-2 mix.

optimum binder content with 75 blows from both ends. The bulk specific gravity (G_{mb}), theoretical maximum specific gravity (G_{mm}) of the mixture, bulk volume of sample, and other volumetric properties were determined for the mix design of the asphalt mixture as shown in Table 3.

The time-temperature viscoelastic response of these mixes was determined using a creep compliance test. The loading in creep compliance test is kept such that the strain in the sample is in the linear viscoelastic regime as discussed in the following section.

4. Viscoelastic characterization of asphalt mixes

The viscoelastic properties of materials are often characterized by analysing their creep behaviour [9]. Creep-related tests are widely used as they offer a straightforward method to distinguish between elastic and viscoelastic strain response [10]. Furthermore, parameters derived from low temperature creep data are utilized to study the initiation and progression of thermal cracking, while those obtained at high temperatures are applied to assess rutting in the service domain [37]. The viscoelastic response is determined using the time-temperature superposition principle based on creep compliance data [9].

4.1. Creep compliance test

The test specimen was prepared according to the volumetric specifications outlined in Section 3.3. Creep compliance testing is applicable to specimens with a maximum aggregate size of 38 mm. According to AASHTO T-322 [38], the specimen should have a 150 ± 9 mm diameter and 38–50 mm height. To ensure smooth and parallel surfaces for accurate mounting of the deformation measurement transducers (LVDTs), 6 mm was trimmed from each end of the sample. Four brass gauge points were affixed to each flat face of the specimen, maintaining a gauge length of 50 mm. On each face, two 0.1 mm LVDTs were mounted—one aligned with the axial loading direction and the other in the lateral direction. More details can be found elsewhere [38]. The strain in the material is kept in the linear viscoelastic range by controlling the applied loading. The test setup for measuring creep compliance is illustrated in Fig. 3.

The creep test at air voids of 4 %, 5 %, and 6 % and three different temperatures of 5°C, 15°C, and 25°C was conducted to study the effect of these parameters on the viscoelastic behaviour of asphalt mixes. The air voids of 4 %, 5 %, and 6 % were achieved by changing

Table 3
Volumetric properties of asphalt mixes obtained from Marshall mix samples.

Mix type	Binder	OBC (%)	G_{mb}	G_{mm}	Air void (%)	VMA (%)	VFB (%)	Stability (kN)	Flow (mm)
BC−2	VG−40	5.70	2.414	2.470	3.887	13.195	70.546	14.216	3.196

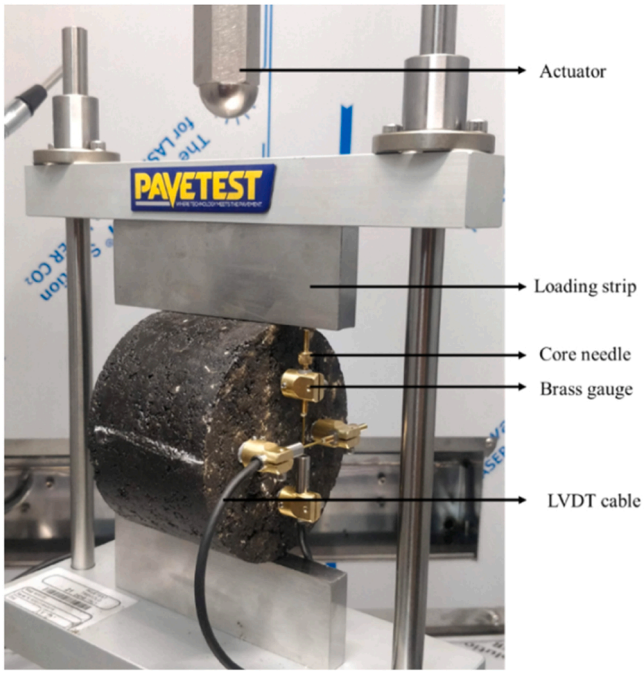

Fig. 3. Specimen loading frame for creep compliance test.

the compactive effort (number of blows) at the same OBC. First of all, a trial number of blows was selected, and air voids were determined. The relation between compactive effort and air voids was established by a curve fitting approach. Based on this relation, compactive effort was evaluated for selected air voids of 4 %, 5 %, and 6 %. The asphalt mix samples were first conditioned at test temperatures of 5°C, 15°C, and 25°C for 3 hours in a temperature-controlled environmental chamber. These samples were then transferred to the dynamic testing system (DTS) for conducting a creep compliance test. The temperature of DTS was set to the test temperatures for every sample. The horizontal and vertical deformations of the specimens at varying temperatures were recorded, as illustrated in Fig. 4.

It was observed that as the loading time increased, both horizontal and vertical deformations also increased. The deformation-time graph showed a steeper gradient at the beginning, which gradually flattened over time. Deformations were further observed to increase with higher air void content and temperature. As the temperature rose, the stiffness of the material decreased, leading to greater deformations. Similarly, an increase in air void content reduced the mix density, allowing the constituent particles to settle more easily into the voids, resulting in greater axial and lateral deformations. It was found that the change in material deformation when temperature changes from 15° to 25° C is significantly higher as compared to the same change in temperature from 5° to 15° C. It indicates the drastic decrease in material stiffness with increasing temperature.

4.2. Material modelling

The Generalized Kelvin Model (GKM) is widely utilized to explain the linear viscoelastic properties of asphalt mixes [39]. It represents the creep compliance data as a series of decaying exponentials, referred to as the Prony series [39]. Viscoelastic functions expressed in the Prony series format can be converted mathematically between the time and frequency domains [39]. The GKM consists of a spring and multiple Voigt elements arranged in series, is more suitable for studying the creep behaviour of viscoelastic materials [39]. The creep compliance, D(t), for the GKM is expressed as [40]:

$$D(t) = D_o + \sum_{k=1}^{n} D_k \left(1 - \exp\left(-\frac{t}{\tau_k}\right)\right) \quad (1)$$

Here, D_o represents equilibrium creep compliance, whereas D_k and τ_k represents creep compliance and relaxation time for the k^{th} element in the series, respectively. A series of constraint optimization processes based on the least square approach is used to evaluate model parameters shown in Eq. 1 [41].

4.3. Conversion of creep compliance to stress relaxation modulus

It is widely recognized that all functions of linear viscoelastic materials are mathematically analogous, with each function encapsulating essentially identical information about the material's relaxation and creep characteristics. Consequently, one type of

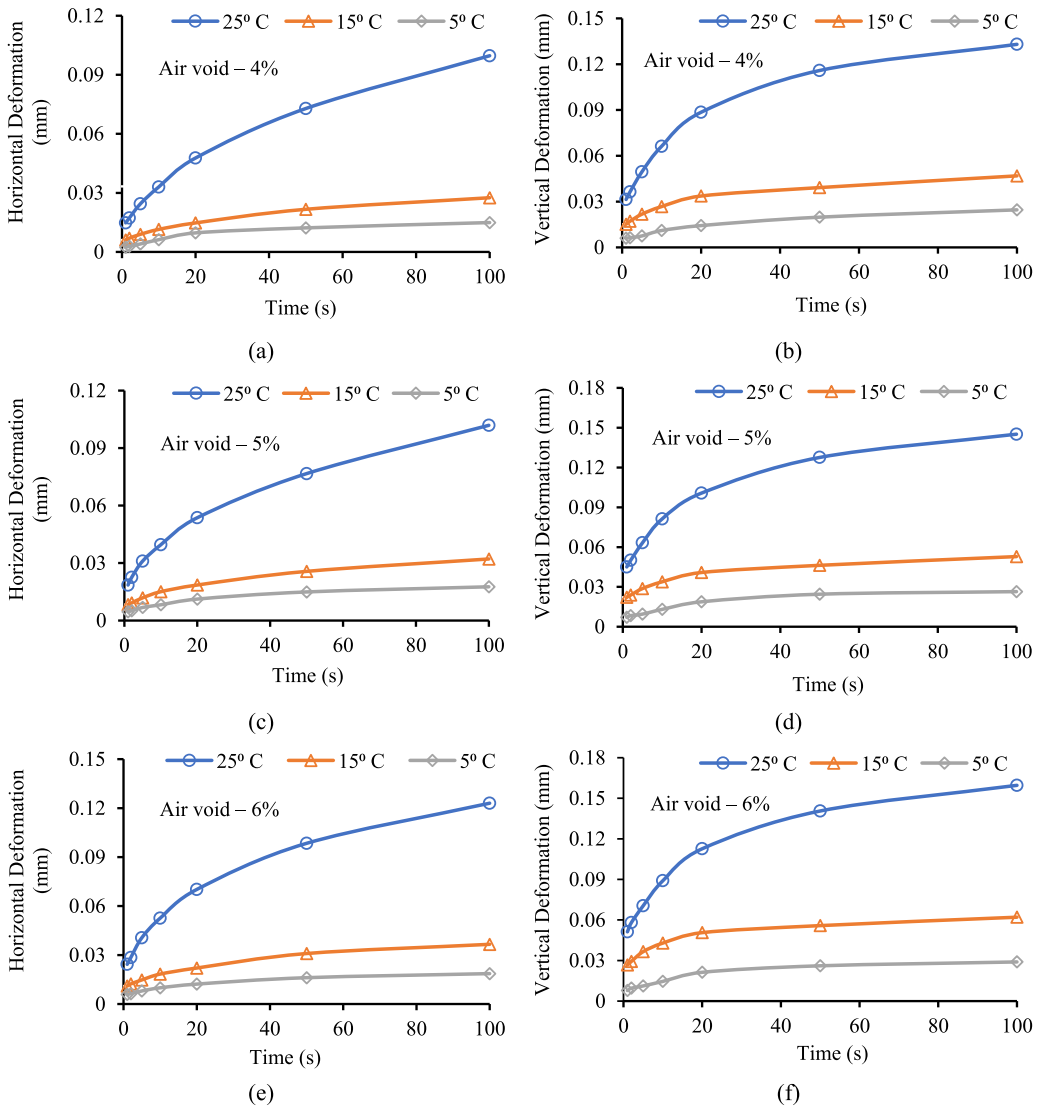

Fig. 4. Deformation-time graph at different air voids and temperatures.

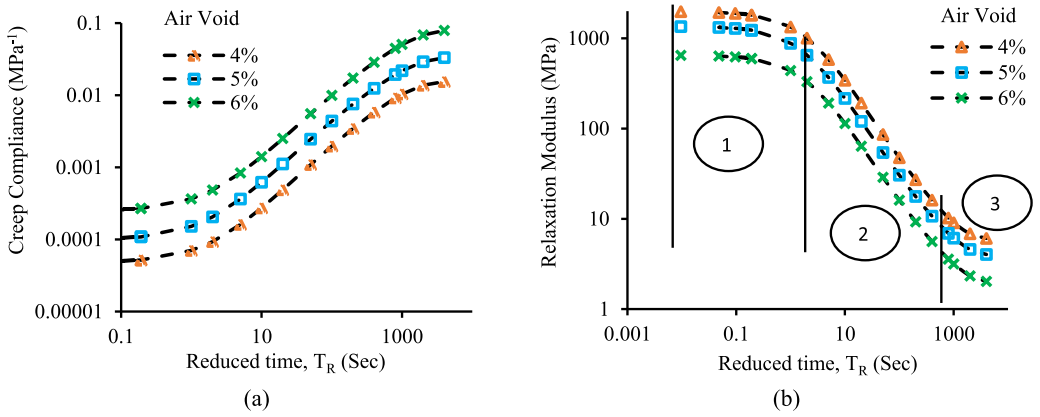

Fig. 5. Prony series fitting of (a) creep compliance and (b) relaxation modulus.

linear viscoelastic material function can be transformed into other types through suitable mathematical operations. The requirement for such interconversions emerges for various reasons. For example, conducting a constant-strain relaxation test on stiff materials can be challenging, whereas executing a constant-stress creep test is typically simpler. In such instances, the relaxation modulus can be derived from the creep compliance via an interconversion method as given below.

$$E(t)D(t) = \frac{\sin(n\pi)}{n\pi} \tag{2}$$

where n is a positive model constant. Derivation of Eq. 2 can be found elsewhere [42]. For an elastic material (n approaches 0), sin (nπ)/nπ approaches to 1. The time-dependent creep response and stress relaxation behaviour have been shown in Fig. 5.

The trends observed in the creep compliance data, when fitted to the Prony series model, were found to closely match those measured in the lab. Therefore, the Prony series model proved to be an effective fit for the creep compliance data, accurately predicting its behavior as a function of time, as shown in Fig. 5(a). In contrast, the relaxation modulus shows an inverse trend compared to the creep compliance over time, as depicted in Fig. 5(b). The relaxation modulus plot can be divided into three distinct zones. Zones 1 and 3 are similar, showing minimal changes in modulus values over time, with the fitting curve being relatively flat. Initially, constituent particles in the mix remain intact and offer maximum resistance to loading, resulting in a higher modulus of the asphalt mix as shown in zone 1. The particles start slipping from their original position as loading time further increases, resulting in a significant reduction in the modulus value in zone 2. When deformation in the mix reaches to maximum limit, any change in relaxation modulus was found negligible, resulting in an almost flat line as shown in zone 3.

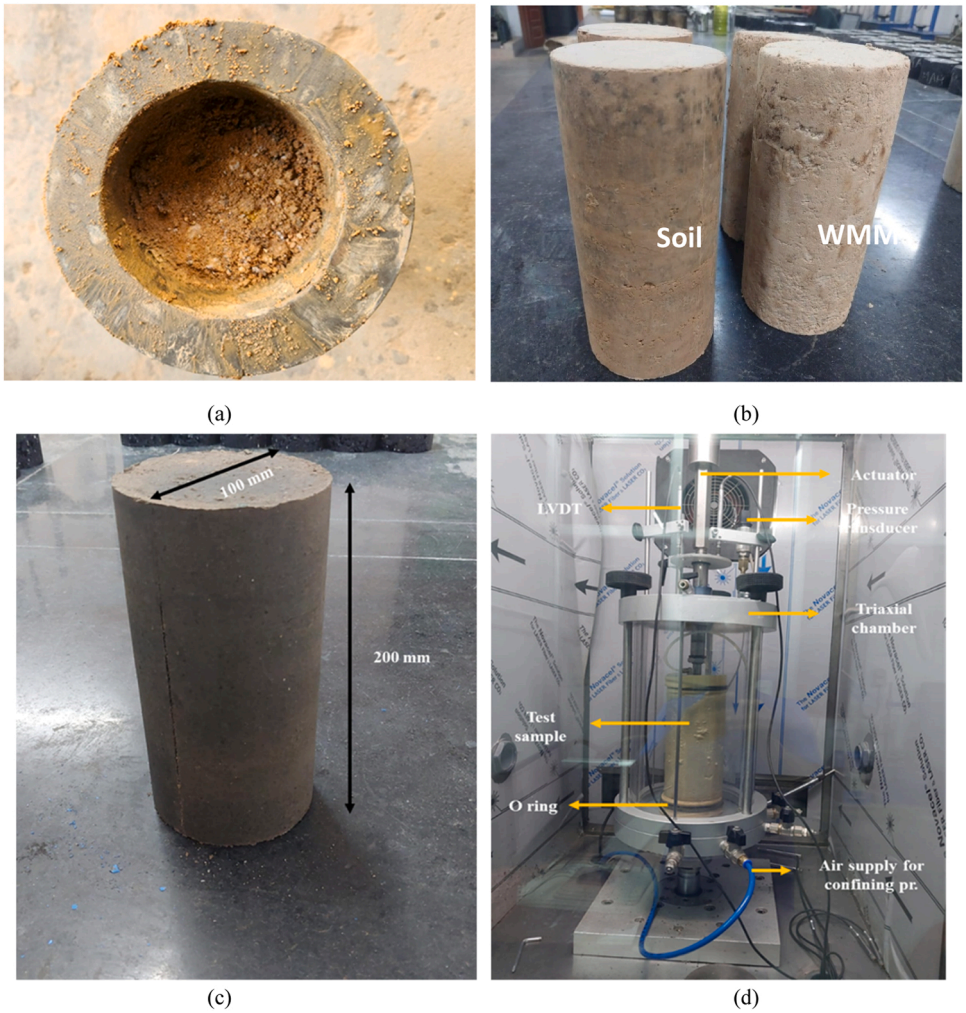

Fig. 6. (a) OMC/MDD determination (b) Compacted samples of soil and aggregates (c) Sample dimensions (d) Triaxial compression test set up.

5. Nonlinear stress-dependent response of UGMs

Aggregates and soil, treated as unbound granular materials (UGMs), are used in the base, subbase, and subgrade layers of the asphalt pavement, serving a crucial role in load distribution. The shear resistance of aggregate skeleton through interlocking of particles gives the bearing capacity to UGMs. With the growing demands on pavement loading and performance, it becomes increasingly vital to deepen our fundamental comprehension of the mechanical behaviour of UGMs and their response to loading. The strain induced in each cycle comprises an elastic strain and a plastic strain. The elastic part of the strain is recoverable on unloading, while the plastic part is permanent. Stress-dependent behaviour of materials used in unbound granular layers is generally evaluated using the resilient modulus (M_r) test [43]. Resilient modulus is the ratio of deviatoric stress (σ_d) to recoverable strain (ε_r). The following section highlights the method of laboratory determination of resilient modulus using repeated load triaxial compression testing.

5.1. Determination of resilient modulus of UGMs

The sample is prepared as per the guidelines of IS 2720 part 8 [44]. The compacted sample at optimum moisture content (OMC), as shown in Fig. 6, is placed in the triaxial compression chamber. A porous bronze disc and specimen cap are placed at the top surface of the sample. The cylindrical sample is enclosed by an elastic rubber membrane to keep it integrated and avoid any material coming out of the chamber. The membrane is then sealed tightly against the cap with the O-ring. Once the test setup in the triaxial chamber is completed, it is connected to the pressure supply line for applying the desired confining pressure.

A repeated axial cyclic stress of load duration 0.1 sec is applied to a cylindrical specimen. The test is conducted using dynamic cyclic stress and a static confining stress applied to triaxial compression chamber as specified by AASHTO T-307 [45]. The sample response in terms of total axial recoverable deformation is measured using a linear variable differential transducer (LVDT) to determine the resilient modulus. Air is used to produce confining stress in the triaxial compression chamber. The haversine-shaped load pulse of duration 0.1 sec and a rest period of 0.9 sec is applied to the test sample. The deformation measuring system consists of two LVDTs fixed to opposite sides of actuator outside the test chamber. These two LVDTs are located equidistant from the actuator.

The resilient modulus test is started by applying 500 repetitions of load cycles equivalent to a maximum axial stress of 27.6 kPa and corresponding cyclic stress of 24.8 kPa in case of soil, and confining pressure is changed to 103.4 kPa and cyclic axial stress to 93.1 kPa for base and subbase materials. This load duration is considered as conditioning period of the test sample. At the end of the conditioning period, if the height of sample is still decreasing, the conditioning period is continued to 1000 load cycles. The conditioning of test sample aids in minimizing the effects of irregular surfaces of the specimen. The drainage valve is kept open to atmospheric pressure throughout the M_r testing. It simulates drained conditions in the asphalt pavement system. Details for the loading sequence for soil (subgrade layer) and aggregates (base and subbase layer) can be found in AASHTO T-307 [45]. The aggregate materials in base and subbase layers are used above the subgrade layer, which is under higher axial stress, so to simulate these conditions, a higher confining and axial stress is applied during M_r test on aggregate materials.

Since fine-grained cohesive soil exhibits stress-softening behavior [14]; so, a decreasing value of confining stress is applied, while the aggregate shows stress-hardening behavior [14], so an increasing confining stress is applied to the sample. The level of confinement in subgrade soil specimens varies from 13.8 kPa to 41.4 kPa, while for aggregates in base and subbase layers, it varies from 20.7 kPa to 137.9 kPa. The variation of confining stress, maximum axial stress, and cyclic stress with loading sequence is shown in Fig. 7 for clarity.

The main difference in loading pattern in the two materials (soil and aggregate) lies in confining stress, as shown in Fig. 7. Stress confinement gradually decreases in soil while it increases in aggregate. Further, the magnitude of confining stress and axial stress is higher in case of aggregate materials as they are expected to carry higher traffic loads than subgrade soil. Traffic load in the pavement structure gradually decreases from the top surface to the lower layers as it distributes over a larger contact area.

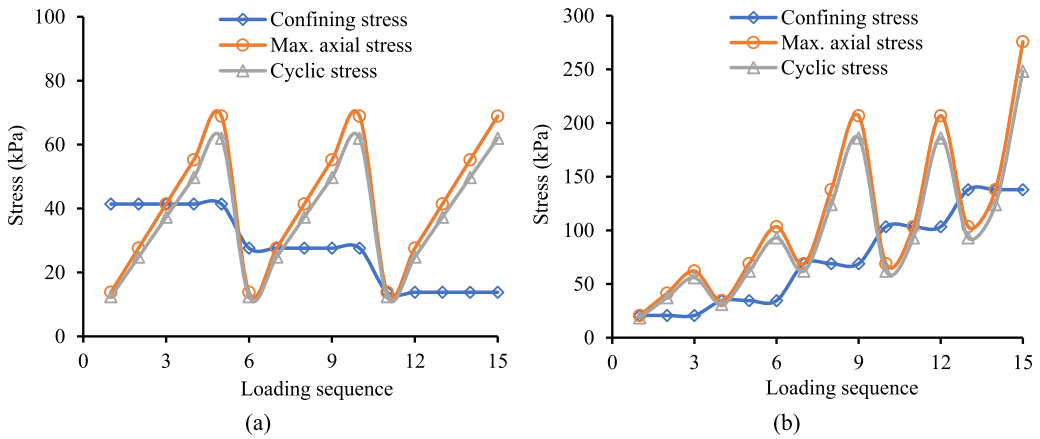

Fig. 7. Test sequence and loading pattern for (a) soil and (b) aggregates.

5.2. Resilient modulus test results

The resilient modulus test was conducted on UGMs (subgrade soil and aggregates) to study the stress-dependent behaviour of these materials. The resilient modulus of UGMs is considered a key parameter in the analyses of asphalt concrete pavement [46–48]. UGMs are characterised based on M_r values, and it is used to evaluate the structural response of the pavement. As discussed earlier, fine-grained cohesive soil shows stress-softening behaviour subjected to repeated cyclic load. It means, as cyclic stress in the material increases, resilient modulus decreases. However, aggregate materials show stress-hardening behaviour, and resilient modulus of the material increases with an increase in the state of stress (cyclic stress). It should be noted that all soil materials do not exhibit stress-softening behaviour. Only fine-grained cohesive soil possesses this peculiar characteristic. The behaviour of other soils (non--cohesive) is different and does not show a fixed pattern.

On the other hand, irrespective of the grade of aggregates used in granular subbase or base layer, it always shows stress-hardening behaviour under the application of repeated cyclic load. The cyclic stress applied in soil material starts from a minimum value of 12.4 kPa and increases to 62.0 kPa in the fifth loading sequence. Loading sequences 1–5 are repeated till the 15th sequence. However, the cyclic stress in aggregate materials is different in all the sequences of loading. The difference in magnitude of maximum cyclic stress is also high for the two materials. The maximum cyclic stress in soil is 62.0 kPa, whereas for aggregate materials, it is 248.2 kPa. The response (M_r) of various soil materials used in this study in the subgrade layer with the change in state of stress (cyclic stress) and loading sequence (excluding the conditioning period) is shown in Fig. 8.

As shown in Fig. 8(a), the response of red soil was found to be similar to that of aggregate materials. The M_r was found to increase with the increase in cyclic stress due to the non-cohesive property of the soil. The fine-grained cohesive soil has a higher plasticity index, which allows for significant plastic flow in the material subjected to repeated cyclic stress. Thus, with the increase in cyclic stress, M_r value decreases as shown in Fig. 8(c) and (d) for fine-grained cohesive soil and black cotton soil. However, non-cohesive materials do not soften under cyclic stress, and plastic flow is insignificant. Any soil that possesses some plasticity and is not completely non-cohesive (cohesive soil mixed with fly ash) may exhibit a combination of stress softening and stress hardening behaviour as shown in Fig. 8(b). Initially, mobilization of plastic flow in the material due to the cohesive property of soil makes it compressible, and M_r decreases for the increase in loading sequence for the first few cycles (5–6 cycles). However, once plastic mobilization is over, further compression of soil requires additional load due to the presence of fly ash in it. So, after a few cycles of loading, M_r of fly ash soil is found to increase further with the increase in load sequence. Similarly, the stress-dependent behavior of aggregate materials in granular subbase (grade V and grade VI) was studied, and variations of M_r with cyclic stress and loading sequence were plotted as shown in Fig. 9.

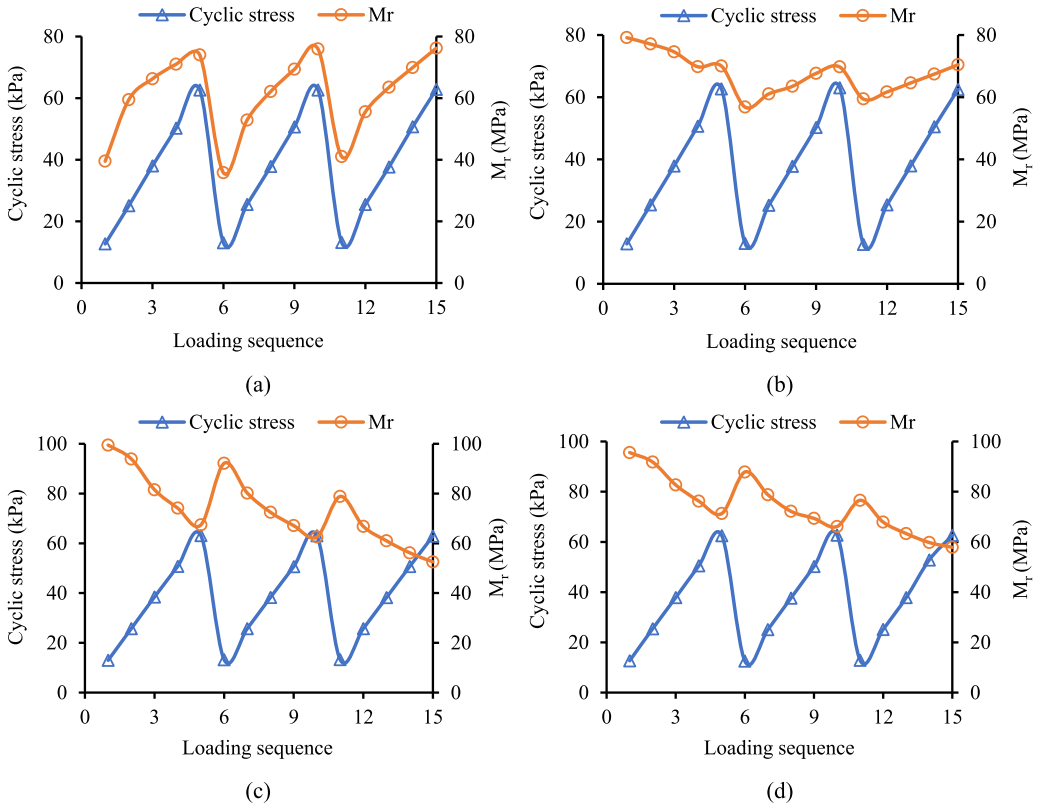

Fig. 8. Stress dependency of resilient modulus with loading sequence (a) red soil (b) fly-ash soil (c) cohesive soil (d) black cotton soil.

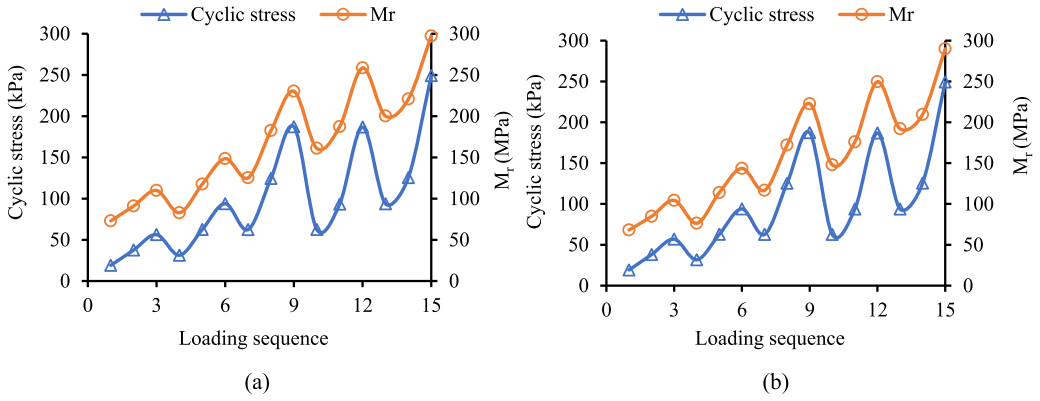

Fig. 9. Stress dependency of M_r with loading sequence for granular subbase (a) grade V and (b) grade VI.

It was found that recoverable strain in the aggregate samples decreases with the increase in cyclic stress, and thus, M_r increases as shown in Fig. 9. It shows stiffness of the material increases as cyclic stress increases, which is the main cause of the stress-hardening behaviour of aggregate materials. The M_r of grade V granular subbase material was found marginally higher than grade VI aggregates. This may be due to a higher percentage of coarser aggregates in grade V granular subbase aggregates. The resilient behaviour of aggregates in a granular base (WMM) was also studied, as shown in Fig. 10.

The resilient behaviour of aggregates in WMM was found similar to granular subbase aggregates, as materials and stress levels are similar in the two cases. These resilient modulus test data were used to model UGMs response in different material models as discussed in the following section.

5.3. *Stress dependent material modelling*

The bilinear model for subgrade soil, whereas the k-Θ model, Uzan model, and the NCHRP model were used to model nonlinear stress-dependent behaviour of unbound granular base and subbase layer materials. Deviatoric stress (σ_d) was first calculated based on axial stress (σ_1) and confining stress (σ_3) obtained from the resilient modulus test. Initially, the model constants were given an assumed seed value, and based on these parameters, M_r values were obtained for different bulk stresses as obtained from experimental results.

5.4. *Hypo-elastic material modelling*

It should be noted that these models (Bilinear, k-Θ, Uzan, Octahedral shear stress model) are empirical relations between M_r and deviatoric stress or bulk stress or shear stress, and thus they cannot be used directly in FE analysis without further assumptions about bulk modulus or Poisson's ratio. So, a constant value of bulk modulus based on the average M_r value obtained from all 15 sequences of loading was considered in this analysis.

Elastic constants (elastic modulus and Poisson's ratio or bulk modulus) are functions of strain invariant (I_1, I_2, *and* I_3), where bulk modulus is assumed constant in the analysis. This assumption makes the relation between volumetric stress and volumetric strain linear as per Hooke's law. This is the important assumption in the hypo elastic modelling. The first strain invariant (I_1) denotes volumetric strain in the sample and it is given as the following constitutive relation:

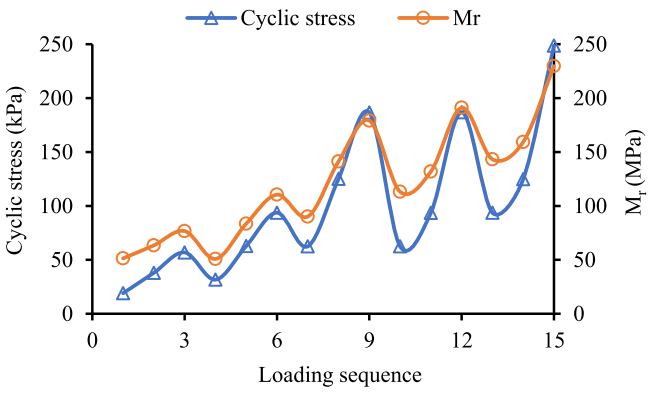

Fig. 10. Stress dependency of resilient modulus with loading sequence for WMM.

$$I_1 = \varepsilon_{vol} = \varepsilon_{11} + \varepsilon_{22} + \varepsilon_{33} \quad (3)$$

$$\sigma_{vol} = K \times \varepsilon_{vol} \quad (4)$$

where, ε_{11}, ε_{22}, $and\varepsilon_{33}$ are principal strains in the material along the principal directions and K is bulk modulus assumed constant. The stress dependency of M_r was plotted against bulk stress for both the experimental and bilinear model in case of subgrade soil and average difference between experimental results and model predicted values is shown in Fig. 11. Results are shown for the four different soils, red soil (RS), Fly-ash soil (FAS), Fine-grained cohesive soil (CS), and Black cotton soil (BCS). The silt content in red soil was relatively higher which made it less cohesive. Fly-ash soil collected near railway tracks was found to have both fly-ash and cohesive soil characteristics. However, black cotton soils are purely cohesive soil, and thus Bilinear model is best fit for fine-grained cohesive as well black cotton soil. The Bilinear model parameters are shown in Table 4.

The average difference in M_r values determined experimentally and predicted from the Bilinear model is highest for red soil and lowest for cohesive soil. It shows the usefulness of the Bilinear model to fit the M_r data for cohesive soils. This model is not suitable for silty soils or other non-cohesive type of soils where some other models must be considered.

The breakpoint modulus (k_1) is a representative parameter of material stiffness. The higher the k_1 value, the higher the M_r. As shown in Table 4, k_1 is highest for black cotton soil and lowest for fly-ash soil, which indicates the highest M_r value for black cotton soil and lowest M_r for fly-ash soil. The stress dependency of M_r for aggregates in base and subbase layers was also determined using repeated load triaxial testing and experimental data were fitted with k-Θ model, Uzan model, and NCHRP model. The M_r data were plotted against bulk stress to study the best fit model as shown in Fig. 12.

Different models (k-Θ model, Uzan model, and NCHRP model) were used to fit M_r test data and compared with experimental results. It was found that the NCHRP model best fits the stress-dependent response of M_r in unbound granular layers (base and subbase layers) whereas, the k-Θ model predicts these responses least reliably. Since the NCHRP model considers the role of octahedral shear stress along with bulk stress in the determination of resilient modulus, it predicts M_r value more reliably. However, the k-Θ model only considers bulk stress dependency of M_r, and a significant difference with experimental results is observed. The Uzan model considers the deviatoric stress instead of octahedral shear stress in the M_r model, which gives a close result to the NCHRP model. It can be concluded that both the Uzan model and the NCHRP model can be used to predict the stress-dependent behavior of UGMs reliably in base and subbase layers.

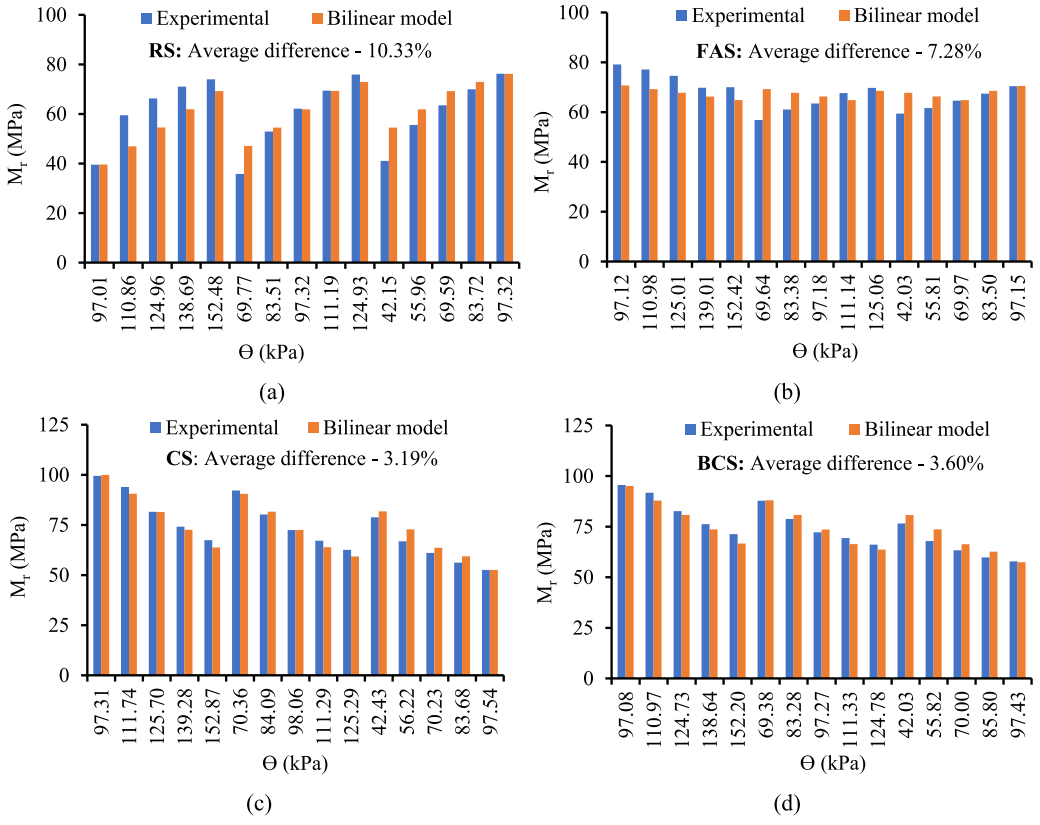

Fig. 11. Bulk stress dependency of M_r fitted with experimental and Bilinear model for (a) Red soil (b) Fly-ash soil (c) Cohesive soil and (d) Black cotton soil.

Table 4
Model parameters for soil used in this study.

Type of soil	Model parameters			
	k_1 (MPa)	k_2 (kPa)	k_3	k_4
Red soil	69.98	29.66	−0.53	−0.23
Fly-ash soil	65.53	21.71	0.10	−0.14
Cohesive soil	73.09	14.34	0.65	0.49
Black cotton soil	92.43	−22.00	0.51	0.44

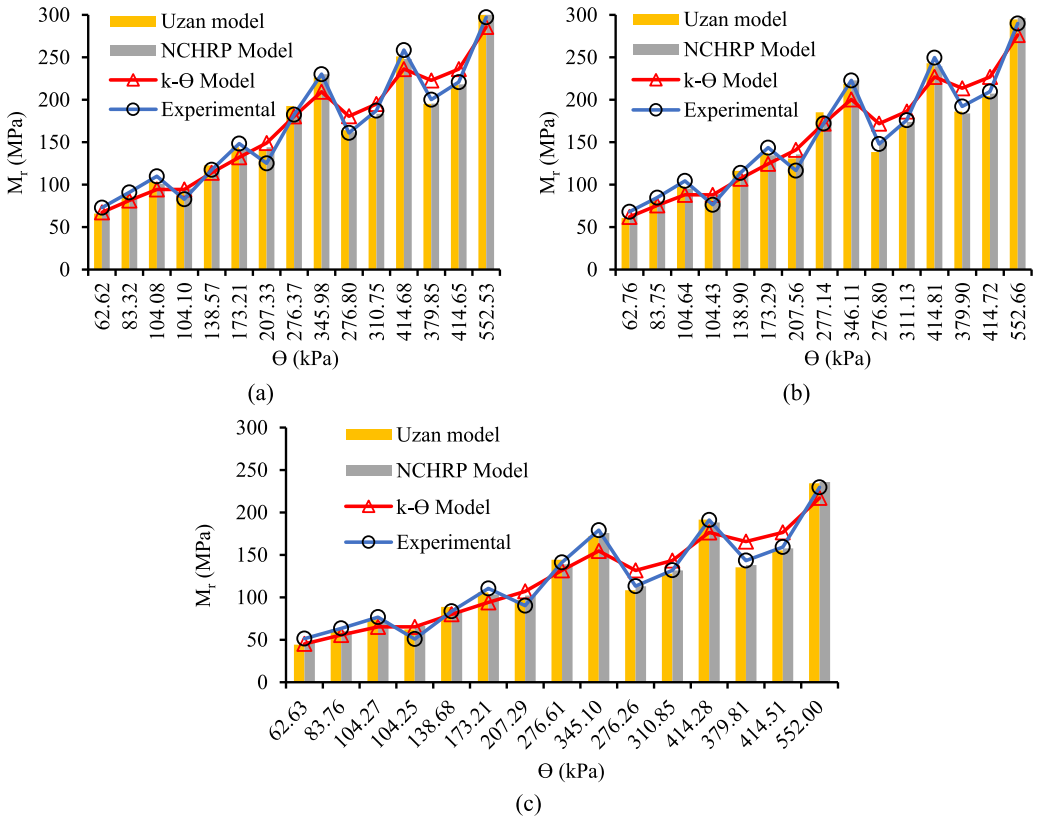

Fig. 12. Variation of M_r with bulk stress for GSB (a) grade V (b) grade VI and (c) WMM.

6. FE modelling of tire-pavement system

Performing research studies in the field is generally labour-intensive, time-consuming, and expensive. Due to advancements in computational facilities in modern days, properly calibrated FE tools have proven to be a good alternative [49]. In this research, a three-dimensional FE model of tire-pavement system using solid tire and deformable AC pavement was developed. The tire was modelled to consider nonuniform contact stress distribution at the tire-pavement interface. The following subsections present a brief description of the developed FE model.

6.1. FE modelling of asphalt pavement

A conventional asphalt pavement system with four layers, AC (wearing and binder course), granular base, subbase, and compacted subgrade layer over natural formation was modelled. FE modelling of asphalt pavement was done using ABAQUS which is capable of handling complex material properties of various layers and nonuniform loading. A pavement of 4 m x 2 m cross section was considered. The thickness of asphalt layer (combined thickness of surface and binder course), base layer (wet mix macadam, WMM), granular subbase layer, and subgrade layer have been kept 150 mm, 300 mm, 350 mm, and 500 mm respectively. A single drainage cum filter layer of granular subbase has been considered in this study. The natural subgrade (foundation) of 6 m thickness below the compacted subgrade layer has been considered as stresses to this depth almost subsides to zero.

The Prony series coefficients as obtained from creep test data were used to define the LVE properties of BC-2 mixes. For defining

stress-dependent response of UGMs, the strain invariant parameters as obtained from hypo-elastic modelling based on repeated load triaxial testing were used in the FE model. The interaction between pavement layers has been defined using surface-to-surface contact. The Penalty friction formulation has been selected to define tangential contact property at the interface of the layers. It makes the simulation more realistic. Penalty formulation considers surfaces in contact as stiff spring that resists surfaces from complete penetration to each other. It allows for small penetration (Δu) of master surface (higher stiffness) to slave surface (lower stiffness). Contact stiffness (K) and restoring forces (F_c as shown in Eq. 5) are calculated to prevent this penetration in each iteration till a permissible penetration value is obtained.

$$\{F_c\} = [K]\{\Delta u\} \tag{5}$$

If the gap between two surfaces in contact is represented by u_n, and Δu_1 and Δu_2 are the sliding distances in lateral directions then the contact traction vector is defined by P and it is given as:

$$P = \begin{cases} 0 if u_n \geq 0 \\ K_n U_n if u_n < 0 \end{cases} \tag{6}$$

The friction coefficient at the interface of the various layers has been determined using Newton's inclined plane test. In this test, a sample specimen of unbound granular layers is compacted at maximum dry density and optimum moisture content while asphalt samples are compacted at design air void. One sample is placed over the other (in order as they are laid in the field during pavement construction) and the inclination of sample placed in a lower position keeps on increasing till the moment sample placed over it just starts sliding. This inclination is noted and tangent of it is recorded as the friction coefficient at the interface. This method has certain limitations as slipping of one layer over the other starts in field under the cyclic loading which has not been simulated in this test. This test may produce friction coefficient values on the conservative side in absence of loading. The other limitation is the lower layer is fixed with the platform which is not allowed to slide over it, however, in field, no layer is completely fixed. So, relative movement of the fixed layer in contact has been ignored. However, this test is easy, convenient, and fast to provides a fair idea of friction between the two surfaces in contact. The details of the measured friction coefficient at the interface of various layers have been shown in Table 5.

The hard contact (fully bonded) was considered to define the normal behaviour of the layer interfaces. The layer of higher stiffness was assigned as master surface while the layer with lower stiffness as slave surface. In the next step, loading and boundary conditions were defined. The axle loading has been simulated using real tire body discussed in a later section. The static loading condition has been simulated in the present study and the magnitude of loading is assigned to the reference node created at the centre of tire body. The boundary conditions used in this study have been discussed separately in a later section. The final step before the solver runs for solving system of equilibrium equations for obtaining the structural response of the asphalt pavement is meshing. In this module, pavement layers and tire are meshed into several parts to generate several elements and nodes in the structure. Meshing discretizes complex geometries into a set of simple and interconnected elements.

6.2. FE modelling of tire

The current design method of AC pavement assumes a circular contact area and uniform distribution of vehicle load, which could significantly differ from the actual field conditions [50,51]. The assumption is used because it simplifies the calculation in pavement analysis. However, it is difficult to explain the behaviour of distresses in AC pavement gradually developing from the surface under heavy vehicles using a simple uniform loading in FE analysis [50,52–54]. Therefore, it is necessary to consider nonuniform contact stress distribution in the FE model. A 3-dimensional test tire was modelled to simulate the complex stress distribution over the loading area. Solid tire in India is generally used in forklift trucks and construction equipment. Solid tires are more popular in heavy-duty vehicles due to their ability to withstand excessive loads and operational capability in harsh environments [55]. It is also easy to evaluate the material properties of solid tire as it consists of single rubber material. For modelling tire rubber, the suitable hyper-elastic material model was obtained using relevant tensile test data and a curve fitting approach [26]. Hyper-elastic models are generally used to calculate elastomer's properties that respond elastically when subjected to large deformations [27]. These material models are expressed in the form of polynomial functions. The generalized strain energy density function for incompressible materials is explained as shown in Eq. 7 below.

$$U = U(F) - P(J-1) \tag{7}$$

where J is determinant of the deformation gradient matrix and U(F) can be expressed as shown in Eq. 8:

$$U(F) = U(I_1, I_2, I_3) = U(\lambda_1, \lambda_2, \lambda_3) \tag{8}$$

Table 5
Friction coefficients at the interface of pavement layers.

S No.	Surface in contact	Sliding angle	Friction coefficient
1	Asphalt concrete – conventional base (WBM)	33.82°	0.67
2	Conventional base (WBM) - subbase	35.75°	0.72
3	Subbase - subgrade	27.47°	0.52

where $I_1, I_2, and\ I_3$ are the first, second, and third strain invariant and $\lambda_1, \lambda_2, and \lambda_3$ are the primary elongation [56]. The Yeoh hyper-elastic material model was selected using the curve fitting method to describe the mechanical behaviour of test tire rubber. The constitutive Yeoh model for compressible rubber is presented in Eq. 9.

$$W = \sum_{i=0}^{3} C_{10}(\overline{I_1} - 3)^i \tag{9}$$

where W is the strain energy density function, $\overline{I_1}$ is the first principal invariant and C_{10} is the material constant. The material constant C_{10} is interpreted as half the initial shear modulus. Table 6 shows the material model constants used in the analysis.

where, C_{10}, C_{20}, and C_{30} are material constants.

6.3. FE modelling of tire-pavement interaction

In this research, the developed model uses contact approaches as proposed by previous researchers [57,58]. As a first step, the contact between the two interacting surfaces of tire-pavement bodies is defined [59]. Both the surfaces (tire and pavement) are considered as deformable, the tire is considered a slave surface whereas the pavement surface is considered a master surface. A finer mesh in the tire region was considered as nodes on the slave surface were not allowed to penetrate the master surface. The interfacial contact was defined using the Penalty function (see Eq. 8) and a tangential contact was defined using the Coulomb friction model as shown in Eqs. 10–11. More details about the contact formulation can be found elsewhere [60].

$$F_n = \left\{ \begin{array}{cc} S_n C & C \leq 0 \\ 0 & C > 0 \end{array} \right\} \tag{10}$$

$$F_t = S_t \delta^e \tag{11}$$

where F_n is the normal interaction force, F_t is tangential interaction force, S_n and S_t are normal and tangential contact stiffness respectively, C is the clearance value of the node in contact relative to the target surface, and δ^e represents elastic deformation of the contact node relative to the target surface.

6.4. Description of element type and boundary conditions

Pavement depth is considered to be 6 m in the vertical direction (-z) to represent the semi-infinite layer below the compacted subgrade as shown in Fig. 13. The depth of 6 m is considered based on the trial depths where vertical stresses subside to zero. The 8-node hexahedral brick element was considered to model pavement layers. A higher number of elements (fine meshing) closer to the loading area and a lesser number of elements (relatively coarser mesh) away from the loading area were considered as shown in Fig. 13. The friction coefficient between pavement surface and tire is kept 0.35 as considered in past studies [61]. The element size in the AC layer closer to the loading area is kept 30 mm× 30 mm while it is 70 mm× 100 mm away from the loading area. In lower layers of the pavement, element size is kept 30 mm× 100 mm closer to loading area while 70 mm× 100 mm away from the loading area. The element size of the outer surface of solid tire is kept 15 mm× 15 mm in this study.

Since a single wheel load has been considered, only half the width of single lane (3.75 m) is required to model. So, a width of 2 m has been considered in the lateral direction. To simulate realistic field constraints, movement of elements in the longitudinal direction (4 m) of AC pavement were constrained as pavement is considered infinite in the longitudinal direction. The elements in the transverse direction (2 m) were also constrained (fixed boundary) as it is supported by the shoulder area. Movement of all the nodes in the vertically downward direction was allowed. The bottom elements of natural foundation were fixed in all degrees of freedom as stress to this depth generally subsides to zero. After defining element types and boundary conditions to the FE model, the problem was submitted for the evaluation of pavement response under the job module. The details of run time and system configuration is given below. Fig. 13 shows the FE model of the tire-pavement system.

Computational time and system configuration: It took approximately 24 minutes to complete single run of the FE analysis on a system of core i7 processor, 16 Gb RAM, 6 Gb graphics, 12 logical processor (s), and CPU speed of 2.60 GHz.

6.5. Validation of FE model

To check the accuracy, the FE model of tire-pavement system was validated using responses obtained from 3D Move Analysis [62] software, a tool specifically developed for analysing layered pavement systems under static/dynamic loading conditions [63,64]. The

Table 6
Coefficients of material model for solid tire.

Material	Coefficients (MPa)		
Rubber	C_{10}	C_{20}	C_{30}
	0.684	−0.022	0.007

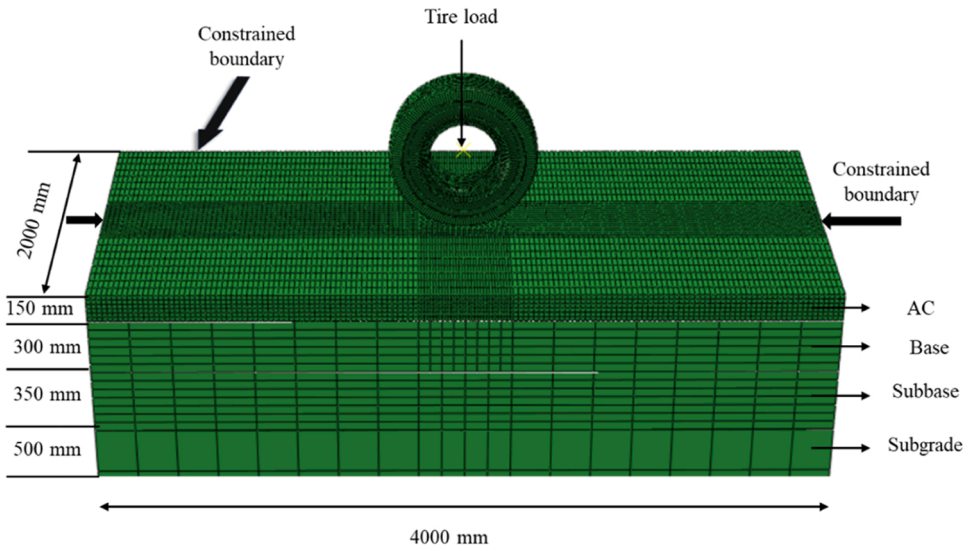

Fig. 13. FE model of tire-pavement system.

3D Move (analytical model) uses a continuum-based finite layer approach to compute pavement responses. This approach treats each pavement layer as a continuum and uses the Fourier transform technique; therefore, it can handle complex surface loadings such as multiple loads and non-uniform tire pavement contact stress distribution. Rate (time/temperature) dependent material properties like viscoelasticity can be accommodated using this approach which makes it a suitable tool to model the asphalt concrete behaviour. Looking into these capabilities, this program was used for validation purpose. Although direct field measurement data were not available, 3D Move Analysis has been widely used and validated against field data in past research, making it a suitable reference for comparative purposes.

The contact area corresponding to different tire loads and maximum vertical deformations in the AC layer were selected as response criteria. The FE simulations were carried out considering the BC-2 mix ($E = 3000$ MPa and $\upsilon = 0.35$) with a conventional base (WMM) layer with identical input parameters for the two analyses considering static loading condition. The considered material properties of unbound materials as obtained from laboratory testing is shown in Table 7.

Fig. 14 shows a comparison of the predicted contact area and maximum AC deformations under different loading levels for the proposed FE model and 3D Move analysis.

As shown in Fig. 14, a good agreement was found between the results obtained from 3D Move Analysis and the proposed FE model. A maximum difference of 5.87 % in the estimated contact area from the two methods as shown in Fig. 14(a) was found. As shown in Fig. 14(b), a maximum difference of 5.37 % in maximum vertical deformation was found. The average difference in contact area was found to be 3.39 % while 2.61 % for maximum deformation. Considering the apparent difference between FE and 3D Move software, the difference can be taken as relatively small. A detailed statistical comparison between the results obtained from ABAQUS and 3D-Move Analysis were done. This includes the coefficient of determination (R^2), root mean square error (RMSE), and mean absolute percentage error (MAPE) for key response parameters (contact area and maximum surface deformation) as shown in Fig. 14. These statistical comparisons between two models, FE based analysis and 3D Move are shown in Table 8.

These results as shown in Table 8 indicate strong correlation and low deviation between proposed FE model and 3D-Move Analysis predictions, confirming the accuracy and reliability of the FE model in simulating asphalt pavement structural responses.

7. Results and discussion

The 3-dimensional FE model of asphalt pavement has been utilized to evaluate the structural response of the asphalt pavement under overloading and tropical climate temperature conditions. Since overloading and high temperature conditions are expected to increase deformations and strains in the pavement, the effect of an increase in layer thickness to limit these strains has also been studied. This analysis can be used to understand whether the consideration of linear elastic properties of materials in various layers

Table 7
Structure of unbound layers and stiffness properties.

S No.	Pavement layers	Thickness (mm)	CBR (%)	M_r (MPa)	υ
1	Subgrade layer	500	10.80	80	0.35
2	Subbase layer	350	NA	295	0.35
3	Base layer	300	NA	295	0.35

NA - Not applicable

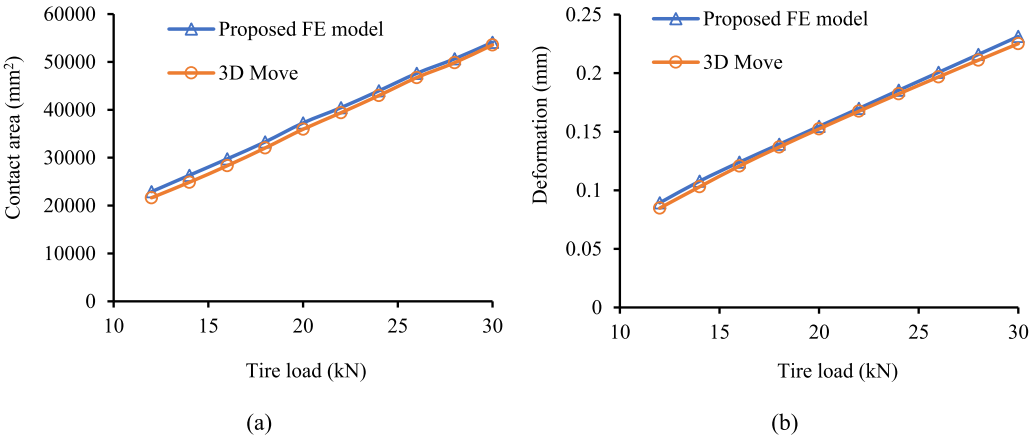

Fig. 14. Variation of (a) contact area and (b) maximum deformation in AC layer with different tire loads.

Table 8
Statistical comparison between proposed FE model and 3D Move Analysis.

Response parameter	R^2	RMSE	MAPE (%)
Contact area (mm^2)	0.942	7.580	3.920
Maximum surface deformation (mm)	0.961	6.280	3.640

underestimates or overestimates pavement strength compared to considering the LVE response of AC and stress-dependent behaviour of UGMs. Since, the LVE response of asphalt material is time dependent; so, it is important to mention here that the pavement response has been recorded immediately after loading (at t = 0 sec). This is also highlighted that these analyses are based on considering static loading conditions. The effect of loading (25–100 % overload compared to standard load for pavement design), air voids in the mix, temperature, and layer thicknesses on structural response and pavement life has been discussed in the following section.

7.1. Effect of loading

The details of loading, its importance, the legal limit, and the concern of overloading for asphalt pavement analysis and design have already been discussed in the previous section. Since linear viscoelastic properties of asphalt mix (BC-2) have been considered in the present simulation, the main idea of the analysis was to find if consideration of viscoelastic properties of these mixes affects pavement life in case of overloading. The standard single axle load of 80 kN (40 kN on one tire) was considered as reference load and overloading of 25–100 % was considered in the analysis. These results will be later compared with the outcomes of the linear elastic case. The analysis will help in understanding the importance of material characterization of asphalt mixes.

The maximum deformation in the pavement and normal strain just below the tire load have been plotted against pavement depth as shown in Fig. 15. The vertical compressive strain (ε_z) and stress (σ_z) at the top of the subgrade layer (z = 800 mm), as well as horizontal tensile strain (ε_t) and stress (σ_t) at the bottom of the asphalt layer (z = 150 mm), has been plotted against loading as shown in Fig. 15 to see the effect of overloading on these critical points.

As shown in Fig. 15 (a), the vertical deformation decreases with an increase in the pavement depth and increases with an increase in the tire load. Maximum vertical deformation is observed at the pavement surface (directly below the tire load) as stress is highest at this point and gradually decreases with the pavement depth as stress disperses to a larger area. An overloading of 25 % from design load of 40 kN on the single tire to 50 kN results in an increase of 21.61 % in vertical deformation in the AC layer (see Table 9). It was further observed that the effect of the increasing load is more significant in the upper layers of the pavement as the load is directly coming over the top surface and reduces significantly after the AC layer. Since, the normal strains with depth under tire load, ε_z, and ε_t are important parameters and are used in pavement performance analysis, variations in these strains are shown in Fig. 15 (b), (c), and (e) respectively. The normal strain is initially tensile up to a depth of about 40 mm due to bending stress in the asphalt layer, gradually compressive strain starts building in the pavement layers. Similar trends were observed for σ_z and σ_t as shown in Fig. 15 (d) and (f). To make ease of understanding, the data of Fig. 15 is presented in tabular form with their respective % changes in Table 9.

As shown in Table 9, the rate of increase of maximum surface deformation with respect to overloading is constant and it was found to increase at a rate of nearly 19.74 % per 25 % of increase in loading. Similar trends were obtained for ε_z and it was found to increase at an average rate of 22.77 % per 25 % of increase in loading. However, the effect of loading on ε_t was not found that significant as in earlier cases. The rate of increase of ε_t was found to be 8.04 % for every 25 % increase in loading. The empirical relations used to evaluate the fatigue life of the asphalt pavement as per the guidelines of IRC:37 is based on ε_t and M_r of asphalt mixes. Since M_r of mixes are based on linear elastic properties so it is difficult to directly correlate these modulus values with the LVE properties of the mixes. Therefore, the fatigue life of the pavement has not been shown in Table 9. However, the rutting life of the asphalt pavement (N_R) is

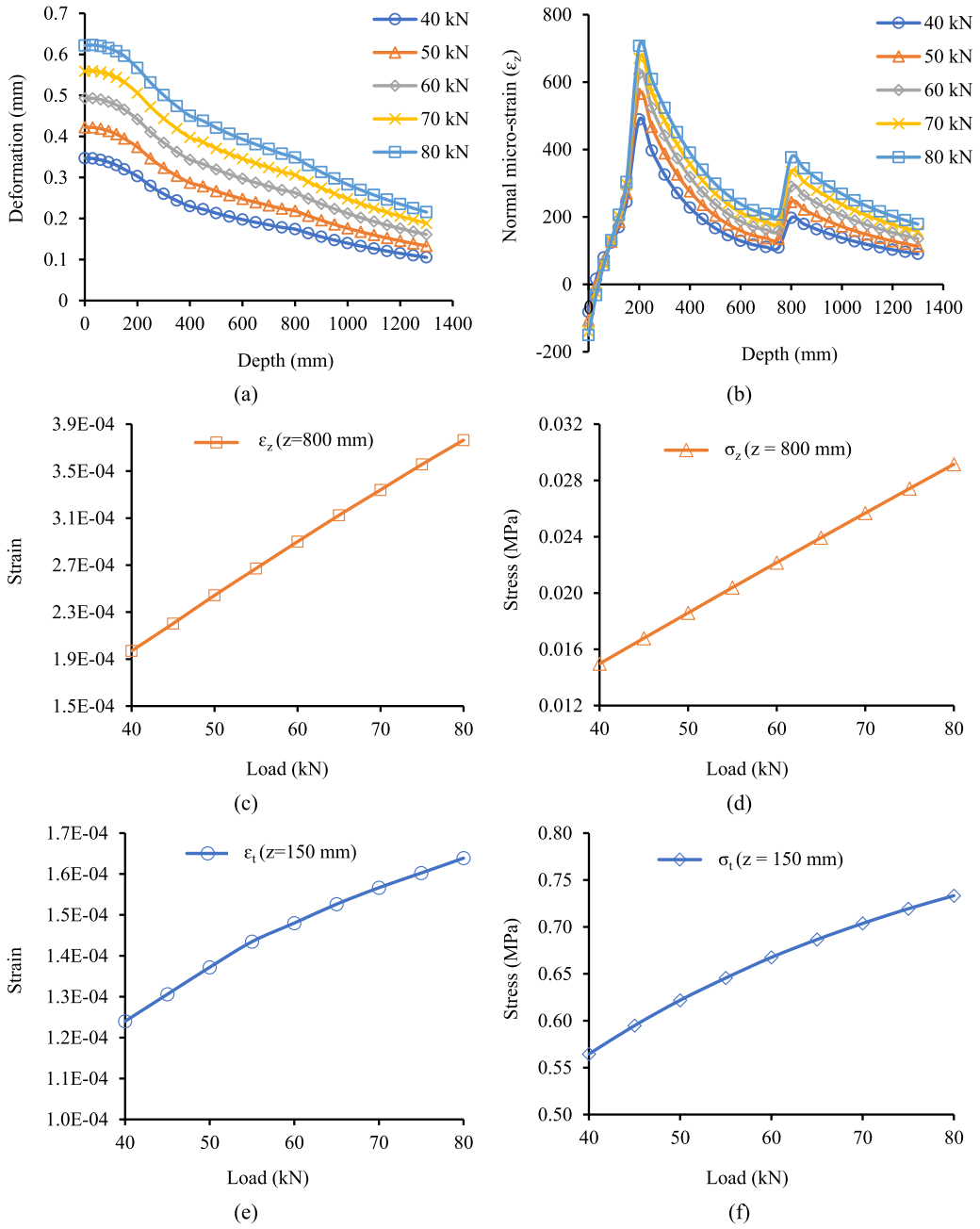

Fig. 15. Effect of loading on LVE response of the pavement.

based on ε_z value only. So, it was evaluated for current LVE simulations as shown in Table 9. It is important to note that, although the average rate of increase of ε_z is 22.77 % only with every 25 % increase in loading, the rutting life of the pavement deteriorates at a much faster rate. For an overloading of 25 % (from 40 kN to 50 kN), N_R reduces by 62.33 %. However, this rate of decrease of N_R keeps on reducing and it was found that for further increase of 25 % loading, the N_R value reduces by 20.36 % only.

7.2. Effect of air voids in the mix

The effort in pavement compaction is important as it decides the final performance. Air voids are generally described as the most effective parameter to explain the behaviour of asphalt mix. Compaction imparts durability and resistance to deformation by locking bitumen-coated aggregate particles together. So, it has a significant effect on the strength and durability of the asphalt mixture. Even within the same air void range, microstructural differences can influence performance. While our study primarily focuses on the

Table 9
Effect of loading on maximum deformation, strains, and pavement life.

Load	40 kN	50 kN	60 kN	70 kN	80 kN
Overloading (%)		25	50	75	100
Maximum deformation	0.347	0.422	0.492	0.559	0.621
% increase in deformation		21.610	41.780	61.090	78.960
ε_z (micro-strains) at top of the subgrade	196.960	244.281	289.979	334.014	376.363
% increase in ε_z		24.025	47.291	69.584	91.086
ε_t (micro-strains) at the bottom of AC	123.993	137.190	148.002	156.505	163.882
% increase in ε_t		10.643	19.363	26.221	32.170
Subgrade rutting life, msa (N_R)	890	335	154	81	47
% reduction in rutting life		62.330	82.696	90.880	94.690

influence of air voids, we recognize that further microstructural or imaging-based investigations could provide deeper insight.

It is well known that, the compactive effort has a huge role in controlling air void in the asphalt mix. During pavement construction, sometimes lack of proper quality control in compaction activity (temperature of asphalt mix is not maintained during laying, lower or higher compactive effort than design) results in different air voids than specified. So, it is important to understand the role of air voids on the structural response of asphalt pavement. The critical pavement response parameters (ε_z and ε_t) ultimately define pavement life in rutting and fatigue. So, it is crucial to evaluate these mechanistic parameters in this study. The variation in vertical deformation and σ_z at three different air voids of 4, 5, and 6 % has been shown in Fig. 16. The σ_z value has been shown on the logarithmic scale as it reduces sharply in a small depth domain. The ε_z and ε_t have also been evaluated to estimate pavement life in rutting and fatigue as shown in Fig. 17. Initially, the ε_z has been determined at various nodal points throughout the pavement depth and later it has been specifically reported at z = 800 mm (top of the subgrade layer) to evaluate rutting life. However, the ε_t value has been evaluated at z = 150 mm (at the bottom of the asphalt layer) only corresponding to 4, 5, and 6 % of air voids in the asphalt mix to evaluate the fatigue life of the pavement.

As shown in Fig. 16, the stress (σ_z) reduction of 71.10, 67.83, and 64.93 % was observed at air voids of 4, 5, and 6 % respectively in the BC-2 layer. It was found that a highr fraction of σ_z is absorbed in asphalt layer itself as stiffness of this layer is relatively much higher than lower layers. The reduction in σ_z in asphalt layer was found higher at lower air void. This is due to a low air void results in more compacted mix and higher stiffness value. The vertical deformation was found maximum at the pavement surface as it falls just below the tire loading and as stress decreases with the pavement depeth, deformation was also found to decrease. As shown in Fig. 16, maximum surface deformation was found to increase by 10.52 and 21.58 % respectively when air void in the asphalt mixture (BC-2) increased from 4 % to 5 % and 6 % respectively. Similar results were obtained for σ_z also. An average increase of 13.34 % and 24.26 % in σ_z value was obtained for the same change in air void as in the previous case. In addition to surface deformation and normal stress, the two critical mechanistic parameters (ε_z and ε_t) were also determined with the help of the FE model to obtain the rutting and fatigue life of the pavement as shown in Fig. 17.

As shown in Fig. 17, the average increase in ε_z value was found to be 13.29 % and 22.56 % when air void in the asphalt mixture rose from 4 % to 5 % and 6 % respectively. The rise in ε_z is higher in lower layers due to increased differences in layer stiffness. The ε_z value at z = 800 mm at an air void of 5 % and 6 % was found 10.15 % and 18.20 % higher than at 4 % air voids. The effect of air void on horizontal tensile strain at the bottom of the asphalt layer was also similar to the results of ε_z. For the same change in air voids, ε_t was found to increase by 9.26 % and 16.88 % respectively. Based on obtained ε_z at different air voids in the asphalt mixes, the subgrade rutting life of the pavement (N_R) was evaluated as shown in Fig. 18.

As shown in Fig. 18, it was found that an increase in air void reduces rutting life of subgrade exponentially. It was found that an increase of 1 % of air void from 4 % to 5 %, reduces N_R by 35.50 %. It is a significant effect on pavement performance considering

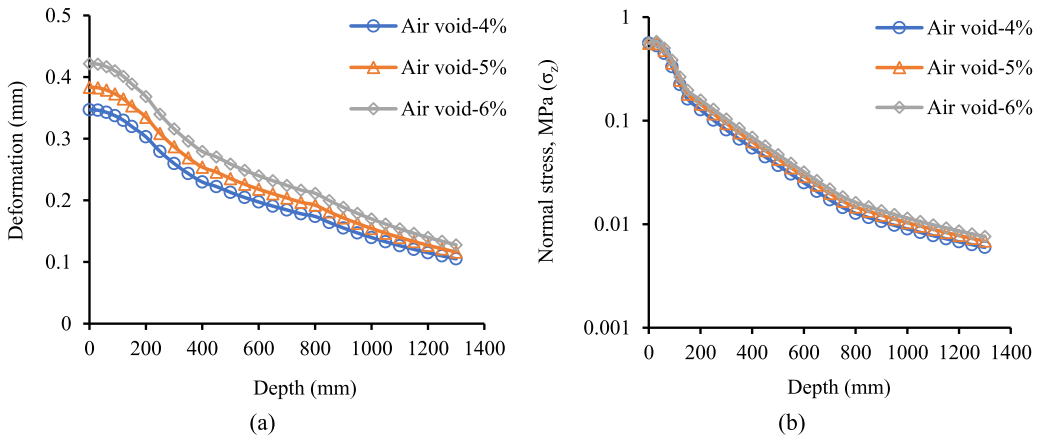

Fig. 16. Effect of air void on (a) deformation and (b) σ_z under LVE simulations.

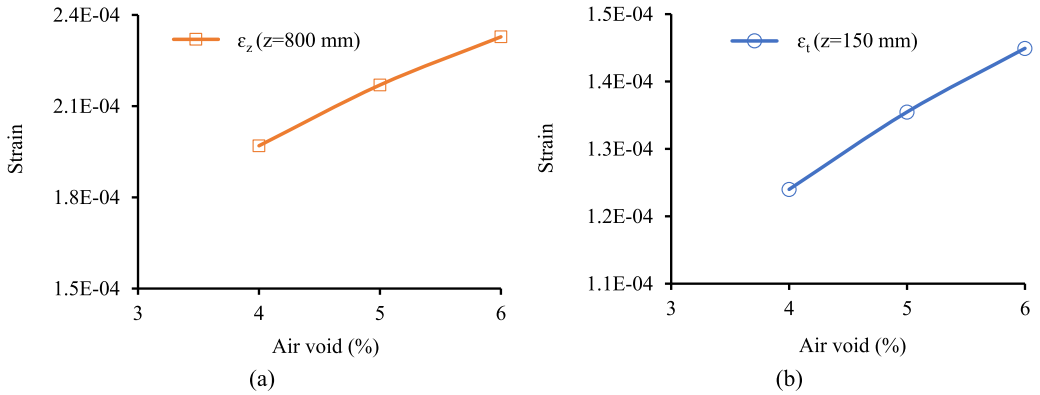

Fig. 17. Effect of air void on (a) ε_z and (b) ε_t under LVE simulations.

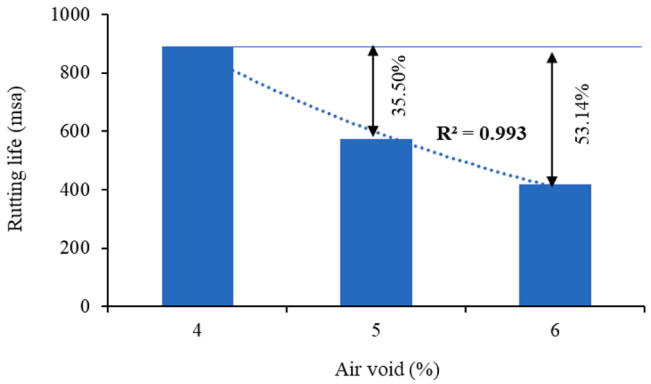

Fig. 18. Effect of air void on rutting life considering LVE properties of AC.

subgrade rutting life. It suggests the importance of quality compaction in the field to meet desired pavement performance.

7.3. Effect of temperature on LVE response of asphalt pavement

The temperature of the asphalt mix is considered one of the major environmental factors that affect pavement performance severely. The damage to asphalt pavement due to a rise in temperature draws the attention of pavement engineers to look at how it affects damage rate (deformation, stress, and strain distribution in pavement layers) in asphalt pavement and how it can finally affect pavement life. Since the asphalt layer is considered viscoelastic, a change in temperature directly affects its modulus value. The subsequent change in asphalt layer modulus modifies the stress distribution in the pavement layers which may lead to loss of pavement life. So, based on local temperature, a suitable grade of binder is selected for the preparation of asphalt mix. The viscoelastic nature of asphalt makes it temperature sensitive and thus has an obvious effect on asphalt rutting, subgrade rutting, and fatigue life. Asphalt layers are prone to thermal and fatigue cracking at low temperatures as they become hard and brittle. However, at higher temperatures, it becomes soft and thus it is more prone to rutting. Since the properties of asphalt mixes change with temperature variation; therefore, their response to axle loading will also be different. The increase in temperature reduces the material stiffness and load-bearing capacity of asphalt mix and thus higher fraction of load-induced stress is transmitted to lower layers which ultimately affects the material response in the base, subbase, and subgrade layer.

Thus, the effect of temperature on the structural response of asphalt pavement, its damage, and performance cannot be ignored and needs a full-scale study. The range of temperature has been selected based on seasonal variation and extreme temperature conditions during winter and summer. Although the highest temperature during summer is below 55° C, the analysis has been extended to 70° C to include maximum surface temperature as discussed in stage II simulation. The Williams-Landel-Ferry (WLF) equation [57] as given by Eq. 12 was used to determine creep compliance data at an extended temperatures of 40, 55, and 70° C.

$$\log(a_T) = -C_1 \times \frac{T - T_R}{C_2 + (T - T_R)} \tag{12}$$

where, a_T is the WLF shift factor, T is the temperature, T_R is the reference temperature selected to construct the creep compliance master curve, and C_1 and C_2 are model constants adjusted to fit the values of the superposition parameter, a_T. This equation can be used

to fit discrete values of the shift factor, a_T vs temperature. The evaluated shift factor and WLF model constants are shown in Table 10.

These shift factors were further used to determine creep compliance data at unknown temperatures of 40, 55, and 70° C as shown in Fig. 19. The experimentally determined creep compliance data at temperatures of 5, 15, and 25° C has already been presented in Section 4.

These creep compliance data were further used to evaluate Prony series constants as discussed in Section 4 to be used as an input parameter in the FE model of asphalt pavement system. The structural response (vertical deformation, normal strain, and horizontal tensile strain) was evaluated using the FE model of the asphalt pavement system (considering a realistic solid tire body) at different test temperatures as discussed earlier. The variation in these structural parameters was obtained with the change in temperature and performance in subgrade rutting and asphalt concrete fatigue was determined. The effect of mix temperature on the structural response (deformation and normal strain) of the asphalt pavement is shown in Fig. 20.

The effect of temperature on pavement deformation and normal strain is significant as shown in Fig. 20 and it needs to be discussed numerically in terms of percentage change to have an exact idea of temperature influence. The maximum surface deformation was found to increase by 13.11, 23.82, 40.55, 73.72, and 118.64 % when the temperature rises from 5° C to 15, 25, 40, 55, and 70° C respectively. At lower temperatures, asphalt mix is stiff and resistance to deformation due to loading is higher. However, as temperature increases, asphalt mix softens due to the viscoelastic behaviour of binder and allows higher penetration into it which leads to higher deformation. It is important to note that, the rate of change in maximum surface deformation at higher temperatures is also high. This is due to the higher loss in asphalt modulus at high temperatures. The reason for higher deformation in lower layers with temperature rise is due to a higher fraction of load-induced stress shared by them. Since, at higher temperatures, the modulus of asphalt layer reduces significantly; thus, the resistance to induced stress is also lower and hence higher fraction of stress is transmitted to lower layers.

Similar trends were obtained for normal strain also. The maximum normal strain was found to increase by 12.78, 27.74, 47.68, 120.69, and 224.55 % respectively when the temperature rises from 5° C to 15, 25, 40, 55, and 70° C respectively. Normal strains in the pavement layers are largely based on vertical deformation and material stiffness of the respective layer. It can be concluded that temperature plays an important role in deciding the type of binder in asphalt mixture and in regions of higher ambient temperature, these mixes shall be characterized based on viscoelastic properties. The LVE characterization of the mixes can more realistically take care of the effect of temperature on mix behaviour.

The critical mechanistic parameters ε_z (z = 800 mm) and ε_t (z = 150 mm) were also evaluated as shown in Fig. 21 to see the effect of temperature on pavement performance in subgrade rutting and asphalt fatigue.

As shown in Fig. 21, ε_z and ε_t follow quadratic variation with temperature. Initially, the slope of the ε_t-temperature graph is positive; however, it seems to become negative at higher temperatures beyond 50° C. It means the tensile strain in the asphalt layer will start decreasing with a further rise in temperature beyond zero slope line. This is important to note that, at higher temperatures near binder's softening point, the resistance to deformation in the mix offered by binder is almost negligible and the mix is viscous and soft which does not allow to develop significant tensile stress in the mix.

The ε_z (z = 800 mm) was found to increase by 12.78, 27.75, 43.79, 54.87, and 63.65 % when temperature rises from 5° C to 15, 25, 40, 55, and 70° C respectively. These variations in ε_z value are slightly higher than average normal strain variations. Since, normal strain includes tensile strain (negative) component also it reduces the overall average ε_z value. The effect of temperature on ε_t (z = 150 mm) was found higher than ε_z (z = 800 mm). The ε_t was found to increase by 15.10, 49.06, 94.35, 166.05, and 198.13 % with the increase in temperature from 5° C to 15, 25, 40, 55, and 70° C respectively. The slope of ε_t-temperature graph is not uniform and keeps on increasing with an increase in temperature which leads to the increasing rate of percentage increase in ε_t value.

These critical mechanistic strain parameters ε_z and ε_t were further used to estimate subgrade rutting and asphalt fatigue life to see the ultimate effect of temperature on pavement performance. Since, this stage of simulation considers LVE properties of asphalt mixes using the creep compliance test, so linear elastic properties (resilient modulus of asphalt mix) are not available. However, the fatigue performance equation as per the guidelines of IRC:37 uses resilient modulus of asphalt mix and tensile strain at the bottom of asphalt layer as an input parameter. The elastic modulus (M_R) of asphalt mix can be determined as a function of pavement temperature as per Eq. 13 [65]:

$$E = 15000 - 7900 \times \log(T) \tag{13}$$

where, E is the elastic modulus of asphalt layer (MPa) and T is the pavement temperature (°C). The elastic modulus was first determined at a test temperature of 5, 15, 25, 40, 55, and 70° C using Eq. 13 as shown in Table 11 and asphalt fatigue life (see Fig. 22) was determined using mechanistic empirical equations as given in IRC:37 [24]. The subgrade rutting life was determined based on ε_z at z = 800 mm as shown in Fig. 23.

As shown in Table 11, the stiffness of asphalt layer (elastic modulus) reduces exponentially with the increase in temperature as a rise in temperature softens the binder present in it leading to reduced resistance to deformation. The ε_t varies with temperature at an increasing rate which results in rapid loss of asphalt fatigue life. The two input parameters (ε_t and M_R) used in the determination of asphalt fatigue life (see Eq. 6.5) are of opposing nature. The ε_t increases with an increase in temperature at one end while the M_r value decreases sharply with the same increase in temperature at another end. Since the effect of temperature on ε_t is significant and it varies with higher power (see Eq. 6.5) than M_R, it becomes a deciding factor in the variation of asphalt fatigue life. As shown in Table 11 and Fig. 22, the fatigue life of the asphalt layer was found to decrease by 29.34, 62.10, 78.40, 86.22, and 84.10 % when temperature increases from 5° C to 15, 25, 40, 55, and 70° C respectively. It was found to vary exponentially. However, this variation changes at higher temperatures and fatigue life were found to increase at 70° C as compared to 55° C. This is due to the rate of change in ε_t reduces

Table 10
Shift factor and WLF constants for various temperatures.

Temperature (°C)	5	15	25	40	55	70
a_T	3.982	1.923	1.000	0.420	0.198	0.102
WLF constants	C_1 – 5.330 and C_2 – 197.635					

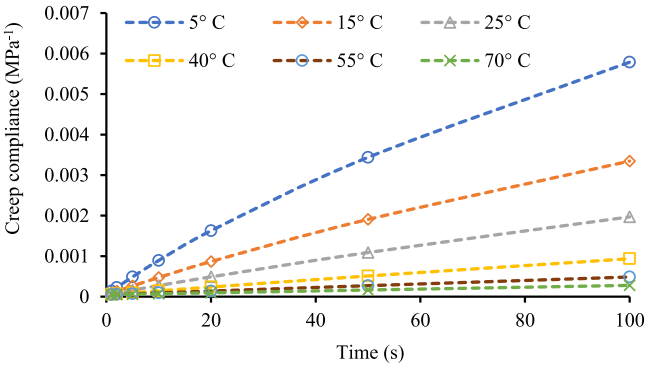

Fig. 19. Time-temperature dependency of creep compliance.

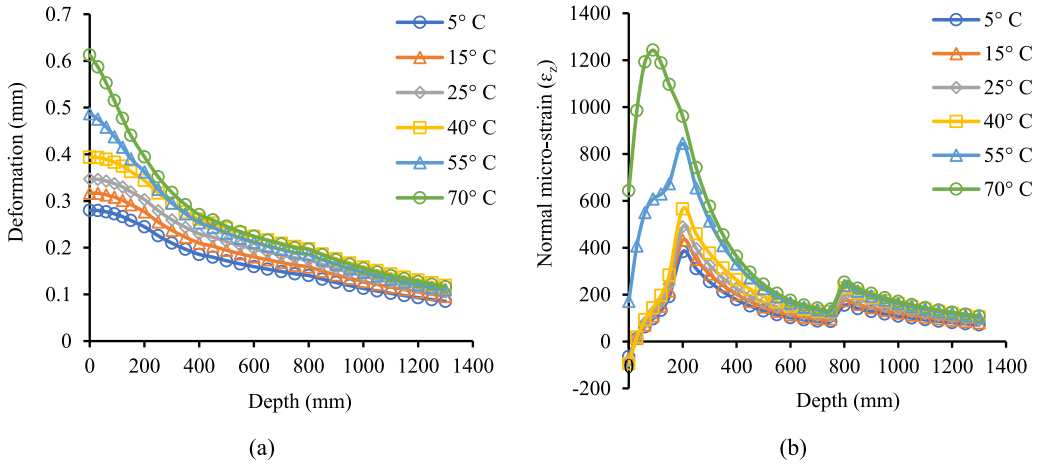

Fig. 20. Effect of temperature on (a) vertical deformation and (b) ε_z under LVE simulations.

at higher temperatures as compared to lower temperatures.

The effect of temperature on subgrade rutting life was found similar to that of asphalt fatigue life. As temperature increases, the stiffness of top layer decreases which results in higher stress transfer to lower layers. This increases the compressive stress and strain in lower layers. The subgrade rutting varies as an inverse power law of ε_z; thus, an increase in ε_z reduces the rutting life of the pavement. It was found that an increase in temperature from 5° C to 15, 25, 40, 55, and 70° C, reduces subgrade rutting life by 42.03, 67.05, 80.73, 86.24, and 89.28 % respectively. This analysis encourages to evaluate temperature-dependent viscoelastic properties of asphalt mixes which can better estimate pavement performance in rutting and fatigue.

7.4. Effect of layer thickness on LVE response of asphalt pavement

The increasing stresses in asphalt pavement due to increased traffic loading results in pavement deformation in a short duration. The structural response of asphalt pavement is often controlled by increasing thickness of various layers mostly the asphalt layer due to higher stiffness. This is considered one of the key solutions to prevent pavement damage during design phase itself. The increase in top layer thickness reduces ε_t and ε_z considerably which results in increased subgrade rutting and asphalt fatigue life. To understand this improvement in pavement life numerically, the thickness of various layers was varied to see its effect on ε_t and ε_z and finally pavement performance.

The asphalt layer thickness in FE simulation was varied from 100 mm to 200 mm while base and subbase layer thickness was varied

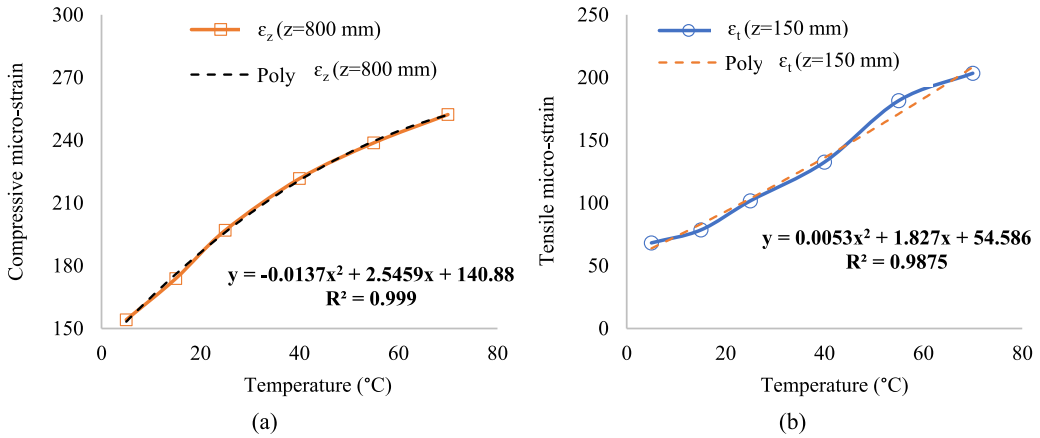

Fig. 21. Effect of temperature on (a) ε_z and (b) ε_t under LVE simulations.

Table 11
Temperature variation of elastic modulus of mixes and fatigue life.

Temperature (°C)	5	15	25	40	55	70
E_{AC} (MPa)	9478.13	5708.88	3956.27	2343.72	1251.13	423.72
ε_t at z = 150 mm (micro-strain)	68.24	78.54	101.72	132.62	181.55	203.44
N_f (msa)	762	680	340	189	95	154

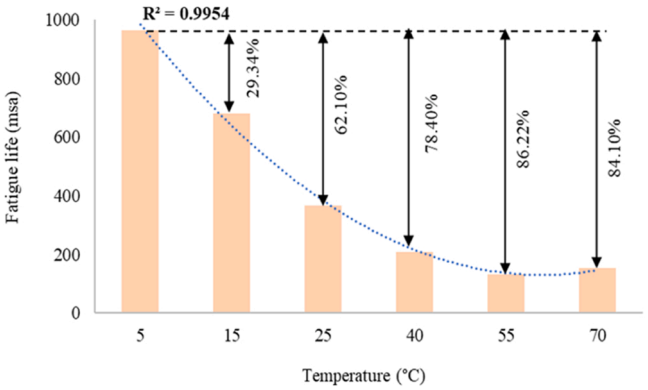

Fig. 22. Effect of temperature on asphalt fatigue life.

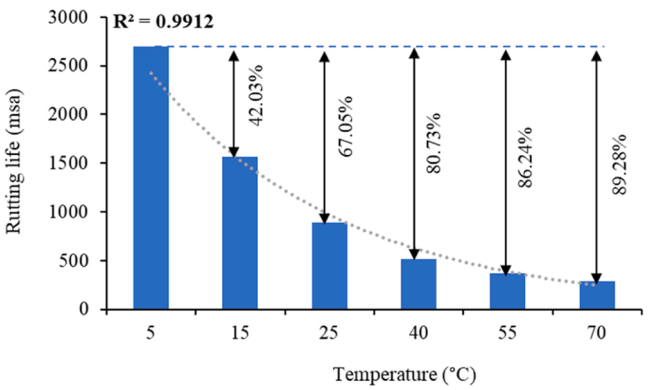

Fig. 23. Effect of mix temperature on subgrade rutting life.

from 150 mm to 310 mm. It shall be noted that the thickness of the asphalt layer is combined thickness of binder and surface course. The range of thickness variation in case of base and subbase layer is based on minimum thickness requirement as specified in IRC:37. The critical mechanistic parameters (ε_z and ε_t) at specific locations as explained earlier were determined as shown in Fig. 24 to further estimate subgrade rutting and asphalt fatigue.

This is important to understand that, a change in asphalt layer thickness has huge potential to limit compressive as well as tensile strain in the pavement. Fig. 24 shows the possible reduction in ε_z and ε_t with the increase in asphalt layer thickness. It was found that the increase in thickness has a higher impact on tensile strain as compared to compressive strain. An average reduction of 7.82 % in ε_z value was obtained for every 20 mm increase in asphalt layer thickness from 100 mm to 200 mm. However, with the similar changes, an average reduction of 11.23 % in ε_t value was obtained. This shows the relative impact of asphalt thickness on ε_z and ε_t values. These are indicative parameters of pavement performance in rutting and fatigue. The other important finding to note that is, change in other lower layer's (base and subbase) thickness has very little effect on compressive strain while having a negligible effect on the horizontal tensile strain. Since ε_t is measured at the bottom of the asphalt layer, any change in the lower layer's thickness practically makes no difference as expected. An average reduction of only 0.33 % in ε_t was found for every 20 mm increase in either base or subbase layer thickness. However, for similar changes, the effect on ε_z was found considerable. An average reduction of 4.36 % in ε_z was found for every 20 mm increase in base or subbase layer thickness from 150 mm to 310 mm. It can be concluded that to limit ε_z, a cost-benefit analysis is required as all the layers have the potential to reduce it significantly. However, to limit ε_t, the option of suitable change in asphalt layer thickness shall be selected.

8. Conclusions

This paper presents a finite element-based framework to consider the time-dependent viscoelastic behaviour of asphalt mixes, the nonlinear stress-dependent response of UGMs, and nonuniform contact stress distribution at tire-pavement interface due to tire loading. This framework can be used by the pavement engineers to predict pavement response under varying conditions of overloading and temperature without actually monitoring it in field which can be cost effective and time saving. It can help in preparing pavement maintenance plan beforehand. The FE model considers complex interactions at layer interfaces using tangential contact properties. The friction coefficients at the layer interfaces were determined using Newton's inclined plate test for better accuracy of the FE model. Overall, this study integrates complex material properties, interface mechanics, and realistic simulation of loading conditions.

The study of linear viscoelastic response of dense graded mixes provides time and temperature-dependent behaviour. The gradient of the deformation-time graph was found to steepen with time at higher temperatures while flattens at lower temperatures. The loading time was found to affect mix response severely. The maximum vertical deformation in BC-2 mix at 2 seconds of loading was found higher by 15.97 % compared to 1 second at 25° C. When this load duration reaches to 100 seconds, the vertical deformation was found to increase by 324.92 %. This gives the relative idea of pavement damage under increased load duration.

The material response under cyclic loading for UGMs was also studied and behaviour of various soil types for the subgrade layer (RS-1, RS-2, FAS, CS, and BCS) to cyclic loading was found different. The RS-1 and RS-2 were found to exhibit stress-hardening behaviour (M_r increases with an increase in cyclic stress) while CS and BCS show stress-softening behaviour (M_r decreases with an increase in cyclic stress). It can be concluded that variation of M_r of a particular soil under cyclic loading is highly dependent on clay content (plasticity) in the material. The FAS was found to exhibit a dual nature of stress softening and hardening behaviour due to the presence of clay soil and fly ash. The aggregate materials in GSB and base layers irrespective of the gradation used were found to exhibit unidirectional stress hardening behaviour to cyclic loading.

The M_r data of GSB and base materials as obtained from repeated load triaxial compression testing were fitted to k-Θ, Uzan, and NCHRP models to explain the nonlinear stress-dependent response of UGMs. The NCHRP model was found to best fit the experimental M_r test data. However, a significant difference in M_r values as obtained experimentally and predicted from the k-Θ model was observed. Since the k-Θ model considers only the bulk stress dependency of M_r, it is not a reasonable fit to M_r response to cyclic

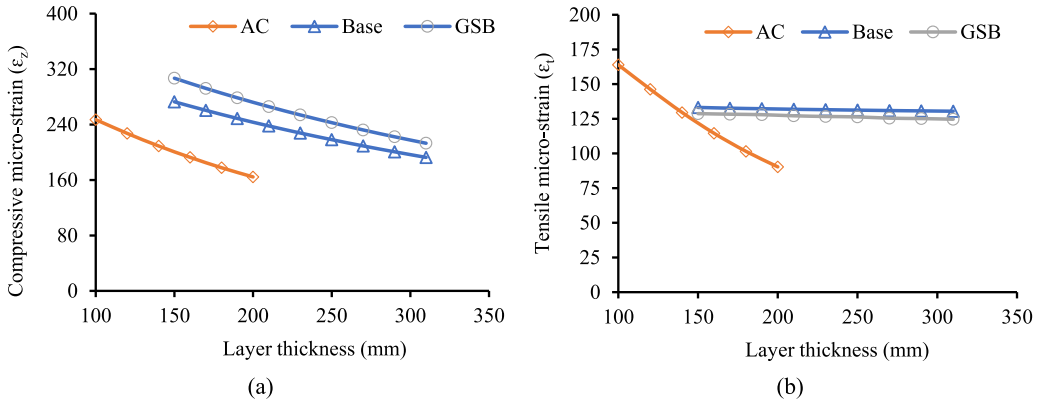

Fig. 24. Effect of layer thickness on (a) ε_z and (b) ε_t under LVE simulations.

loading. The stress-dependent response of soil material was fitted using the Bilinear model. A good agreement with experimental data (average difference of 3–4 %) was found in the case of fine-grained cohesive soil. However, the Bilinear model is not a good fit for the stress-dependent response of other soils which are not purely cohesive (an average difference of 7–11 % was obtained).

These complex material properties of asphalt mixes and UGMs were finally simulated using the FE model to evaluate pavement response under overloading and variable temperature conditions, especially in tropical regions like India. The results demonstrated that overloading has a huge impact on pavement damage. The resistance to subgrade rutting reduces significantly in case of overloaded vehicle. A similar damaging effect was also observed in case of variation in mix temperature. A rise in temperature reduces mix stiffness and thus its M_r which results in higher compressive strain at the subgrade top and the rutting life of the subgrade is affected severely. The asphalt fatigue life was found to reduce by 29.34 % for a rise in mix temperature by 10° C from 5 to 15° C.

9. Limitations and future scope of study

Present study considers static loading conditions likely to underestimate asphalt pavement strength and its life compared to realistic field conditions where the load duration is small. Also, the obtained response of the asphalt pavement using proposed finite element-based framework needs to be validated using extensive study of field performance of pavement under similar conditions.

In future studies, transient loading can be considered to simulate more realistic loading conditions in field. The LVE response of asphalt pavement can be explored for gap graded mixes like stone mastic asphalt as these mixes are commonly used in high temperature climatic conditions as rut resistant layer. Present study considers single rubber material for simplifying FE modelling of solid tire. However, other components, like bead, carcass, ply, sidewall, reinforcement, etc., can be further considered to integrate and model pneumatic tires.

CRediT authorship contribution statement

Gupta Ankit: Writing – review & editing, Supervision, Resources, Methodology, Investigation, Conceptualization. **Kumar Abhinav:** Writing – original draft, Visualization, Validation, Software, Methodology, Funding acquisition, Formal analysis, Data curation, Conceptualization. **Premarathna W.A.A.S.:** Visualization, Software, Data curation. **Anupam Kumar:** Writing – review & editing, Visualization, Supervision, Methodology, Investigation, Conceptualization.

Declaration of Competing Interest

The authors declare the following financial interests/personal relationships which may be considered as potential competing interests: Abhinav Kumar reports financial support was provided by Ministry of education, Government of India. Abhinav Kumar reports a relationship with Indian Institute of Technology BHU Varanasi that includes: non-financial support.

Data Availability

Data will be made available on request.

References

[1] S. Helwany, J. Dyer, J. Leidy, Finite-element analyses of flexible pavements, J. Transp. Eng. 124 (5) (1998) 491–499, https://doi.org/10.1061/(ASCE)0733-947X (1998)124:5(491).
[2] MoRTH, Specifications for road and bridge work (Fifth revision),” New Delhi, 2013.
[3] Roberts, F.L., Kandhal, P.S., Brown, E.R., Lee, D.Y., & Kennedy, T.W. (1996). Hot mix asphalt materials, mixture design and construction, Transportation Research Board.
[4] A. Graziani, F. Cardone, A. Virgili, Characterization of the three-dimensional linear viscoelastic behavior of asphalt concrete mixtures, Constr. Build. Mater. 105 (2016) 356–364, https://doi.org/10.1016/j.conbuildmat.2015.12.094.
[5] R. Luo, H. Liu, Y. Zhang, Characterization of linear viscoelastic, nonlinear viscoelastic and damage stages of asphalt mixtures, Constr. Build. Mater. 125 (2016) 72–80, https://doi.org/10.1016/j.conbuildmat.2016.08.039.
[6] Y. Zhang, B. Birgisson, R.L. Lytton, Weak form equation–based finite-element odelling of viscoelastic asphalt mixtures, J. Mater. Civ. Eng. 28 (2) (2016) 04015115, https://doi.org/10.1061/(ASCE)MT.1943-5533.
[7] H. Di Benedetto, F. Olard, C. Sauzéat, B. Delaporte, Linear viscoelastic behaviour of bituminous materials: from binders to mixes, Road. Mater. Pavement Des. 5 (sup1) (2004) 163–202, https://doi.org/10.1080/14680629.2004.9689992.
[8] G.D. Airey, B. Rahimzadeh, A.C. Collop, Viscoelastic linearity limits for bituminous materials, Mater. Struct. 36 (2003) 643–647, https://doi.org/10.1007/BF02479495.
[9] L. Zhang, X. Zhang, X. Liu, Y. Luo, Viscoelastic model of asphalt mixtures under repeated load, J. Mater. Civ. Eng. 27 (10) (2015) 04015007, https://doi.org/10.1061/(asce)mt.1943-5533.0001256.
[10] M.W. Witczak, T.K. Pellinen, M.M. El-Basyouny, Pursuit of the simple performance test for asphalt concrete fracture/cracking, J. Assoc. Asph. Paving Technol. (2002) 71.
[11] Wardle, L.J. (1977). A Computer Program for the Analysis of Multiple Complex Circular Loads on Layered Anisotropic Media.
[12] M. Kim, E. Tutumluer, Modeling nonlinear, stress-dependent pavement foundation behavior using a general-purpose finite element program, Pavement Mech. Perform. (2006) 29–36.
[13] B. Saad, H. Mitri, H. Poorooshasb, Three-dimensional dynamic analysis of flexible conventional pavement foundation, J. Transp. Eng. 131 (6) (2005) 460–469, https://doi.org/10.1061/(ASCE)0733-947X(2005)131:6(460).
[14] M. Kim, E. Tutumluer, J. Kwon, Nonlinear pavement foundation modeling for three-dimensional finite-element analysis of flexible pavements, Int. J. Geomech. 9 (5) (2009) 195–208, https://doi.org/10.1061/(ASCE)1532-3641(2009)9:5(195).
[15] S.F. Brown, Soil mechanics in pavement engineering, Géotechnique 46 (3) (1996) 383–426, https://doi.org/10.1680/geot.1996.46.3.383.

[16] Thom, N.H., & Brown, S.F. (1988). The effect of grading and density on the mechanical properties of a crushed dolomitic limestone. In Australian Road Research Board (ARRB) Conference, 14th, 1988, Canberra (Vol. 14, No. 7).
[17] Rowshanzamir, M.A. (1995). Resilient cross-anisotropic behaviour of granular base materials under repetitive loading (Doctoral dissertation, UNSW Sydney).
[18] Tutumluer, E. (1995). Predicting behavior of flexible pavements with granular bases. Georgia Institute of Technology.
[19] S.F. Brown, J.W. Pappin, Analysis of pavements with granular bases (810) (1981).
[20] J. Uzan, Characterization of granular material, Transp. Res. Rec. 1022 (1) (1985) 52–59.
[21] M.R. Thompson, R.P. Elliott, ILLI-PAVE based response algorithms for design of conventional flexible pavements, Transp. Res. Rec. 1043 (1985) 50–57.
[22] Witczak, M.W., & Uzan, J. (1988). The universal airport pavement design system, Report I of IV: Granular material characterization. University of Maryland, College Park, MD.
[23] H.S. Yu, M.Z. Hossain, Lower bound shakedown analysis of layered pavements using discontinuous stress fields, Comput. Methods Appl. Mech. Eng. 167 (3-4) (1998) 209–222, https://doi.org/10.1016/S0045-7825(98)00120-0.
[24] IRC 37-2018, Guidelines for the design of flexible pavements (Fourth Revision)," New Delhi, Nov. 2018.
[25] Williamson, M.J. (2015). Finite element analysis of hot-mix asphalt layer interface bonding. Kansas State University.
[26] Premarathna, W.A.A.S., Jayasinghe, J.A.S.C., Wijesundara, K.K., Ranatunga, R.R.M.S.K., & Senanayake, C.D. (2020). Performance comparison of solid tires and non-pneumatic tires using finite element method: Application to military vehicles.
[27] Y. Li, W.Y. Liu, S. Frimpong, Effect of ambient temperature on stress, deformation and temperature of dump truck tire, Eng. Fail. Anal. 23 (2012) 55–62, https://doi.org/10.1016/j.engfailanal.2012.02.004.
[28] IS 1206: 1978. Methods for Testing Tar and Bituminous Materials, Viscosity Test. Bureau of Indian standards, New Delhi, India.
[29] A. Mittal, K. Arora, G. Kumar, P.K. Jain, Comparative studies on performance of bituminous mixes containing laboratory developed hard grade bitumen, Adv. Civ. Eng. Mater. 7 (2) (2018) 92–104, https://doi.org/10.1520/ACEM20170039.
[30] IS 73, Paving bitumen – specification, Bur. Indian Stand., N. Delhi, India (2013) (2013) 1–4 (April).
[31] A. Singh, A. Gupta, M. Miljković, Intermediate-and high-temperature damage of bitumen modified by HDPE from various sources, Road. Mater. Pavement Des. 24 (sup1) (2023) 640–653, doi: 10.1080/ 14680629.2023.2181017.
[32] ASTM D6373, Standard Specification for Performance-Graded Asphalt Binder, West Conshohocken.
[33] IS 1203, 2022, Methods for Testing Tar and Bituminous Materials — Determination of Penetration. Bureau of Indian standards, New Delhi, India, pp. 1–10.
[34] IS 1205: 1978. Methods for Testing Tar and Bituminous Materials, Softening Point Test. Bureau of Indian standards, New Delhi, India.
[35] IS 2386-1, 1963: Methods of Test for Aggregates for Concrete, Part I: Particle Size and Shape. Bureau of Indian standards, New Delhi, India.
[36] IS 2386-4, 1963. Methods of test for aggregates for concrete, Part 4: Mechanical properties. Bureau of Indian standards, New Delhi, India.
[37] Jeong, M. (2005). Comparison of creep compliance master curve models for hot mix asphalt (Doctoral dissertation, Virginia Tech).
[38] T. AASHTO, 322-03, Determining the Creep Compliance and Strength of Hot-Mix Asphalt (HMA) Using the Indirect Tensile Test Device. American Association of State Highway and Transportation Officials, Washington D.C., USA, 2005, pp. 1–11.
[39] Y. Zhao, Y. Ni, W. Zeng, A consistent approach for characterising asphalt concrete based on generalised Maxwell or Kelvin model, Road. Mater. Pavement Des. 15 (3) (2014) 674–690, https://doi.org/10.1080/14680629.2014.889030.
[40] N.W. Tschoegl. The Phenomenological Theory of Linear Viscoelastic Behavior: an Introduction, Springer Science & Business Media, 2012.
[41] S.K. Srirangam, Numerical Simulation of Tire-pavement Interaction 53 (2015) 9.
[42] S.W. Park, Y.R. Kim, Interconversion between relaxation modulus and creep compliance for viscoelastic solids, J. Mater. Civ. Eng. 11 (1) (1999) 76–82, https://doi.org/10.1061/(ASCE)0899-1561(1999)11:1(76).
[43] S.H. Kim, K. McFall, J. Kwon, J. Yang, J.H. Jeong, Use of linear viscoelastic theory to predict resilient behavior of unbound granular materials, KSCE J. Civ. Eng. 20 (2016) 1806–1812, https://doi.org/10.1007/s12205-015-0129-2.
[44] IS 2720 – Part 8, Determination of water content-dry density relation using heavy compaction, Bur. Indian Stand., New Delhi, India (1994) 1–14.
[45] AASHTO T307-99, Determining the resilient modulus of soils and aggregate materials, 2007.
[46] R. Ji, N. Siddiki, T. Nantung, D. Kim, Evaluation of resilient modulus of subgrade and base materials in Indiana and its implementation in MEPDG, Sci. World J. 2014 (1) (2014) 372838, https://doi.org/10.1155/2014/372838.
[47] Kolisoja, P. (1997). Resilient deformation characteristics of granular materials (pp. 188-201). Finland, Publications: Tampere University of Technology.
[48] NCHRP, (2004). Guide for Mechanistic-Empirical Design Of New and Rehabilitated Pavement Structures, Part2, Washington DC, USA.
[49] A. Kumar, T. Tang, A. Gupta, K. Anupam, A state-of-the-art review of measurement and modelling of skid resistance: the perspective of developing nation, Case Stud. Constr. Mater. 18 (2023) e02126, https://doi.org/10.1016/j.cscm.2023.e02126.
[50] X. Jiang, C. Zeng, X. Gao, Z. Liu, Y. Qiu, 3D FEM analysis of flexible base asphalt pavement structure under non-uniform tyre contact pressure, Int. J. Pavement Eng. 20 (9) (2019) 999–1011, https://doi.org/10.1080/10298436.2017.1380803.
[51] R.S. Dwyer-Joyce, B.W. Drinkwater, In situ measurement of contact area and pressure distribution in machine elements, Tribol. Lett. 14 (1) (2003) 41–52.
[52] Y. Oubahdou, E.R. Wallace, P. Reynaud, B. Picoux, J. Dopeux, C. Petit, D. Nélias, Effect of the tire–pavement contact at the surface layer when the tire is tilted in bend, Constr. Build. Mater. 305 (2021) 124765, https://doi.org/10.1016/j.conbuildmat.2021.124765.
[53] De Beer, M., Fisher, C. and Jooste, F.J., 2002, August. Evaluation of non-uniform tyre contact stresses on thin asphalt pavements. In Ninth international conference on asphalt pavements (Vol. 5, pp. 19-22).
[54] R.V. Siddharthan, N. Krishnamenon, M. El-Mously, P.E. Sebaaly, Investigation of tire contact stress distributions on pavement response, J. Transp. Eng. 128 (2) (2002) 136–144, doi: 10.1061/ ASCE0733-947X2002128:2136.
[55] J. Phromjan, C. Suvanjumrat, A suitable constitutive model for solid tire analysis under quasi-static loads using finite element method, Eng. J. 22 (2) (2018) 141–155, https://doi.org/10.4186/ej.2018.22.2.141.
[56] M. Hossain, P. Steinmann, More hyperelastic models for rubber-like materials: consistent tangent operators and comparative study, J. Mech. Behav. Mater. 22 (1-2) (2013) 27–50, https://doi.org/10.1515/jmbm-2012-0007.
[57] K. Anupam, T. Tang, C. Kasbergen, A. Scarpas, S. Erkens, 3-D thermomechanical tire–pavement interaction model for evaluation of pavement skid resistance, Transp. Res. Rec. 2675 (3) (2021) 65–80, https://doi.org/10.1177/0361198120963101.
[58] W.A.A.S. Premarathna, J.A.S.C. Jayasinghe, K.K. Wijesundara, P. Gamage, R.R.M.S.K. Ranatunga, C.D. Senanayake, Investigation of design and performance improvements on solid resilient tires through numerical simulation, Eng. Fail. Anal. 128 (2021) 105618, https://doi.org/10.1016/j.engfailanal.2021.105618.
[59] S.A. Shoop, Finite Element Odelling of Tire-terrain Interaction, University of Michigan, 2001.
[60] H. Wang, I.L. Al-Qadi, I. Stanciulescu, Simulation of tyre–pavement interaction for predicting contact stresses at static and various rolling conditions, Int. J. Pavement Eng. 13 (4) (2012) 310–321, https://doi.org/10.1080/10298436.2011.565767.
[61] A. Gupta, S.K. Pradhan, L. Bajpai, V. Jain, Numerical analysis of rubber tire/rail contact behavior in road cum rail vehicle under different inflation pressure values using finite element method, Mater. Today.: Proc. 47 (2021) 6628–6635, https://doi.org/10.1016/j.matpr.2021.05.100.
[62] M. Nasimifar, S. Thyagarajan, N. Sivaneswaran, Backcalculation of flexible pavement layer moduli from traffic speed deflectometer data, Transp. Res. Rec. 2641 (1) (2017) 66–74, https://doi.org/10.3141/2641-09.
[63] A. Kumar, A. Gupta, K. Anupam, V.P. Wagh, Finite element-based framework to study the response of bituminous concrete pavements under different conditions, Constr. Build. Mater. 417 (2024) 135368, https://doi.org/10.1016/j.conbuildmat.2024.135368.
[64] A. Kumar, A. Gupta, K. Anupam, A. Singh, S. Premarathna, Mechanistic empirical studies of emulsion stabilized bases using finite element method, Mech. Based Des. Struct. Mach. (2025) 1–28, https://doi.org/10.1080/15397734.2025.2491033.
[65] A.E.A.E.M. Behiry, Fatigue and rutting lives in flexible pavement, Ain Shams Eng. J. 3 (4) (2012) 367–374, https://doi.org/10.1016/j.asej.2012.04.008.